POLITECNICO DI TORINO

DEPARTMENT OF MECHANICAL AND AEROSPACE ENGINEERING

Thesis for master's degree in mechanical engineering

Towards Active Flow Control by Means of Plasma Actuators

By Mehrdad Nikkhou

Supervisor: Prof. Jacopo Serpieri

Co-Supervisor: Gaspare Li causi

July 2025

Abstract

The transition from laminar to turbulent flow in boundary layers significantly affects aerodynamic performance, drag, and fuel efficiency in aerospace applications. This study presents a numerical investigation into the use of Dielectric Barrier Discharge plasma actuators as an active flow control method to delay transition and reduce drag. A physics-based body force model based on the Shyy [38] formulation was implemented via User Defined Functions in ANSYS Fluent to simulate plasma actuation effects.

A series of simulations were conducted on a flat plate configuration using the transition SST model to validate baseline transition behavior against NASA benchmark data. Parametric studies were then performed to assess the influence of key actuator parameters, including electric field strength and electrode positioning, on boundary layer stability and transition onset. The results indicate that in turbulent intensity of 0.03%, activating DBD Plasma actuators promotes transition in boundary layer and even changing actuator position or electric field strength won't be helpful. At turbulent intensity of 1%, actuators were able to delay boundary layer transition. In turbulent intensity of 5%, actuators were unable to have a significant effect on boundary layer transition.

To identify optimal actuation configurations, a Multi-Objective Genetic Algorithm (MOGA) was employed. Actuator electric field strength and position were input variables for this optimization while intermittency selected as output function. Further enhancement was achieved by investigating a dual-actuator configuration, demonstrating improved flow control through combined momentum injection. The study confirms that properly tuned plasma actuators offer a viable AFC strategy for aerodynamic optimization. The findings contribute to the design of more efficient actuator configurations for practical integration in aerodynamic systems.

Acknowledgments

First and foremost, I would like to express my deepest gratitude to my supervisor, Professor Jacopo Serpieri, for his exceptional guidance, unwavering support, and insightful mentorship throughout the course of this thesis. His expertise and encouragement have been fundamental to the progress and quality of my work. I am also sincerely thankful to Gaspare Li Causi, whose technical advice, constructive feedback, and generous support played a crucial role in the development of this research. His patience and willingness to assist me at every stage of the project are deeply appreciated. My heartfelt thanks go to the Flow Control and Aeroacoustics Group at Politecnico di Torino for fostering a collaborative and stimulating research environment. Finally, I am profoundly grateful to my family for their unconditional love, encouragement, and belief in me. Their support has been my greatest source of strength throughout this academic journey, and I dedicate this achievement to them.

Table of Contents

List of Figures

List of Tables

Chapter 1: Introduction

The aviation industry has experienced significant changes in fuel consumption patterns, influenced by technological advancements, regulatory pressures, and economic considerations. As airlines strive for greater fuel efficiency, a range of strategies and models have been developed to optimize fuel use across various phases of flight. Fuel consumption remains a critical concern in aviation, accounting for nearly 40% of operational costs and playing a major role in environmental sustainability. Aerodynamics has a considerable effect on fuel consumption, as it directly impacts drag and overall aircraft performance. Enhancing aerodynamic efficiency, particularly during cruise flight where drag is a dominant factor, can lead to substantial reductions in fuel burn.

Among the components of aerodynamic drag, skin friction drag is particularly important. It results from the shear stress exerted by the fluid on the surface of a moving body and significantly influences fuel efficiency and emissions. Skin friction drag contributes approximately 20–40% of the total drag experienced by vehicles moving through fluids, underscoring its importance in fuel consumption. This type of drag is affected by several parameters, including boundary layer thickness, percentage of chord flow separation, surface texture (e.g., shark skin vs. polished surfaces), and whether the flow is laminar or turbulent. The Reynolds number plays a pivotal role in these dynamics [1].

Figure 1 illustrates the effect of Reynolds number on the drag coefficient. It is evident that turbulent flow is associated with a higher range of drag coefficients compared to laminar flow. Therefore, to reduce skin friction drag in aircraft, it is advantageous to maintain laminar flow over the wings and other primary surfaces contributing to overall drag. The transition from laminar to turbulent flow is predominantly governed by the Reynolds

number (Re), a dimensionless parameter representing the ratio of inertial to viscous forces in a fluid. For boundary layer flow over a flat plate, this transition typically occurs at a Reynolds number of approximately 500,000, although it is also influenced by factors such as surface roughness, free-stream turbulence intensity, and pressure gradient.

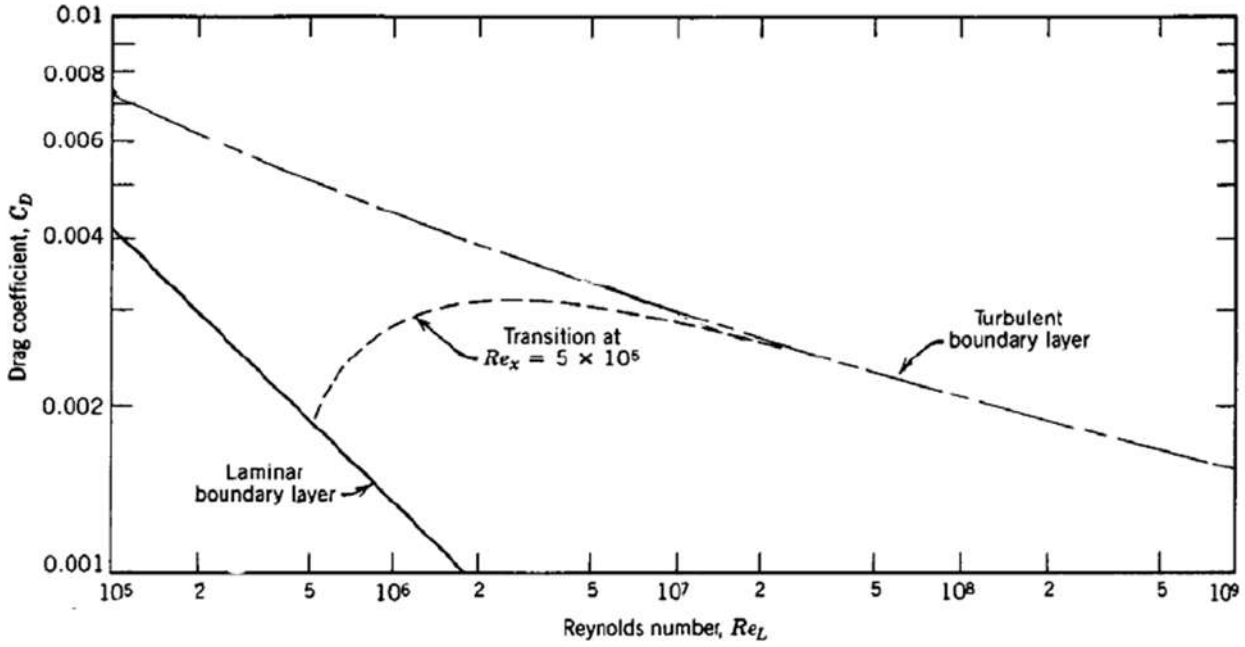

Figure 1 - Drag Coefficient Vs Reynolds Number

Flow control methods (Figure 2) can be broadly categorized into active and passive techniques. Passive flow control relies on fixed structural modifications or surface treatments that influence the flow environment without requiring any external energy input. In contrast, active flow control involves dynamic interventions that require energy, typically in the form of electrical, mechanical, or pneumatic input, to manipulate the flow.

Active flow control strategies have shown to effectively manage the transition from laminar to turbulent flow. These methods are designed to modify boundary layer behavior by either delaying or promoting the onset of turbulence, depending on the desired aerodynamic outcome. Notable active techniques include plasma actuators, acoustic excitation, Lorentz

Forces, synthetic jets, localized surface heating or cooling and harmonic blowing and suction, each offering distinct mechanisms and advantages across different flow regimes.

While active methods provide real-time control and adaptability, passive flow control approaches are simpler and do not require energy input or feedback loops. Examples of passive techniques include surface temperature regulation, structural shaping, and the application of surface roughness to influence boundary layer stability and flow separation characteristics.

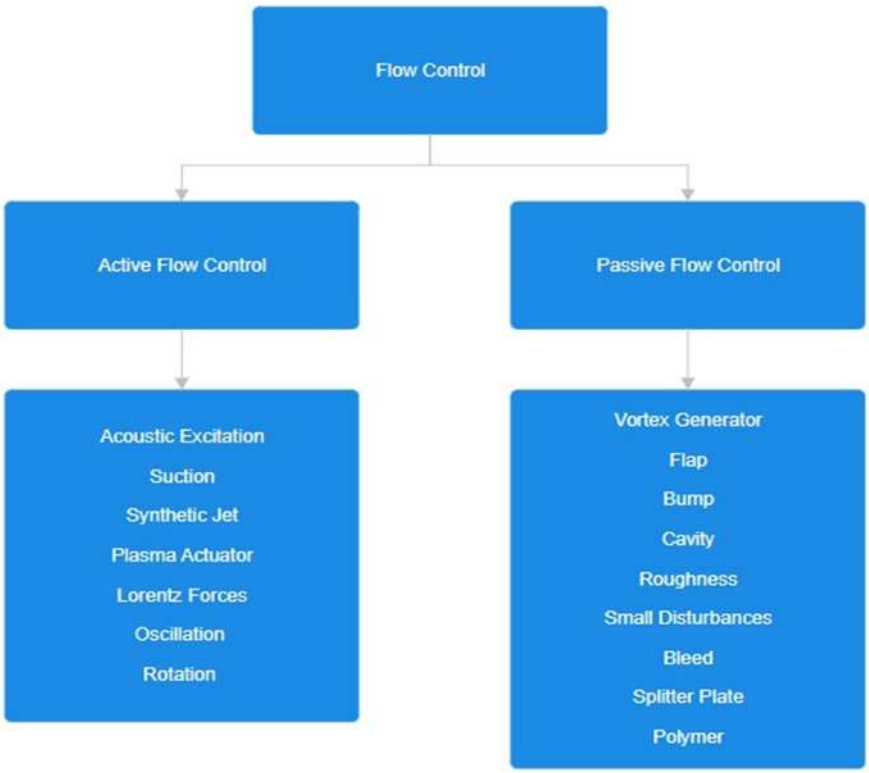

Figure 2 - Flow Control Methods

Plasma actuators, particularly those based on Dielectric Barrier Discharge (DBD) technology, have garnered significant attention in recent decades as efficient, fast-response, and non-intrusive devices for active flow control.

These actuators are capable of generating a localized body force within the flow field, enabling precise manipulation of boundary layers, turbulence characteristics, and overall aerodynamic behavior, without the need for mechanical components. Owing to their ability to induce flow instabilities, delay or accelerate transition, and influence flow separation, plasma actuators have been widely applied in areas such as aerodynamic drag reduction, noise mitigation, and lift enhancement.

The fundamental working principle of a DBD plasma actuator (Figure 3) is based on the ionization of air molecules under the influence of a strong electric field. The actuator is typically composed of two electrodes: one exposed to the surrounding air and the other embedded beneath a dielectric material. When an alternating high voltage is applied across the electrodes, a plasma discharge forms along the edge of the exposed electrode. This discharge region contains charged particles (ions and electrons), which collide with neutral air molecules, transferring momentum and producing a localized body force. This force accelerates the near-wall airflow, thereby altering the local flow dynamics and enabling effective flow control.

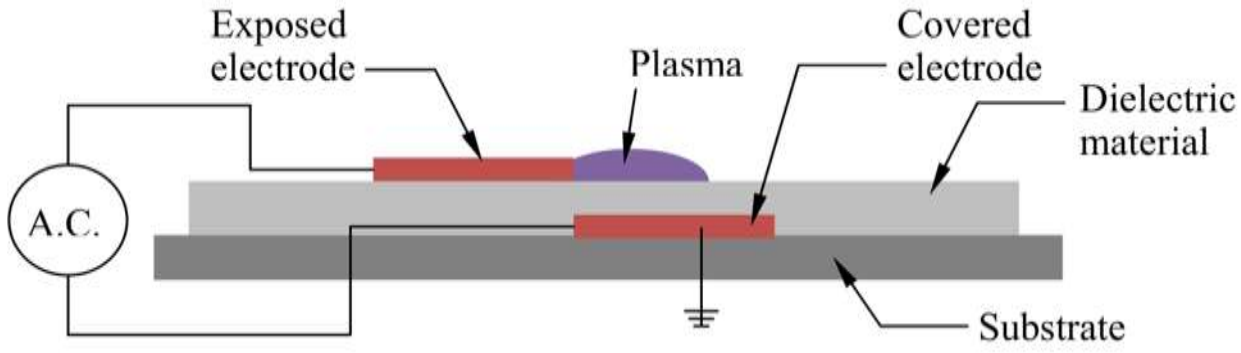

Figure 3 - Schematic of a Dielectric Barrier Discharge (DBD) Plasma Actuator Configuration

The objective of this study is to investigate the key parameters influencing the fluid dynamics of plasma-actuated flow. Parameters such as the actuator's voltage, operating frequency, and electrode separation distance have a significant impact on the characteristics of the plasma discharge and its interaction with the flow. A thorough understanding of these effects is

essential for the development of effective flow control strategies aimed at delaying the laminar-to-turbulent transition over a flat plate.

In the final phase of the study, an optimization framework is established to systematically optimize selected input parameters with respect to predefined performance metrics. This approach enables the identification of actuator configurations that maximize control effectiveness while maintaining practical constraints on energy input and system integration.

Outline

This thesis begins in **Chapter 2** with a comprehensive literature review of the laminar-to-turbulent transition mechanisms and the key factors influencing this process. Additionally, various flow control methods, both passive and active, are discussed in detail, along with their practical applications. In **Chapter 3**, we develop a solid theoretical foundation by exploring the governing equations of fluid motion and the physics of plasma actuators. This chapter also introduces the numerical models used to simulate plasma-induced body forces and outlines the implementation strategy using ANSYS Fluent, including the integration of a User Defined Function (UDF) for active flow control. **Chapter 4** presents the simulation results and offers a detailed analysis of how different actuator parameters affect boundary layer behavior, transition location, and flow characteristics. An optimization framework is constructed to identify the most effective actuator configurations. The methodology employs a response surface model and a Multi-Objective Genetic Algorithm (MOGA) to explore the design space and evaluate performance metrics such as intermittency and skin friction. Finally, **Chapter 5** summarizes the findings of the study and provides concluding remarks, along with recommendations for future research directions.

Chapter 2: Literature Review

2.1 Laminar-to-Turbulent Transition

The transition from laminar to turbulent flow is a fundamental phenomenon in fluid dynamics that has a profound impact on aerodynamic performance, heat transfer, and drag characteristics. In a laminar boundary layer, fluid particles move in smooth, orderly layers with minimal mixing. However, due to various instability mechanisms, this structured motion can deteriorate into turbulence, leading to increased skin friction and enhanced mixing effects [2].

The transition process typically occurs in several distinct stages. Initially, the flow is in a receptive state, making it highly sensitive to external disturbances such as surface roughness, acoustic waves, and free-stream turbulence. These disturbances introduce small perturbations into the boundary layer, which may grow under the influence of linear instability mechanisms. In low-speed flows, these instabilities often manifest as Tollmien-Schlichting (TS) waves, while in curved geometries, Görtler vortices can dominate [3]. The amplification of these disturbances is strongly influenced by the Reynolds number, with higher values typically leading to earlier onset of transition [4].

As the amplitude of these disturbances increases, nonlinear interactions begin to dominate. This leads to the formation of vortical structures and secondary instabilities, which cause a rapid transfer of energy across different disturbance modes, accelerating the breakdown of the orderly flow. Eventually, the flow undergoes turbulent breakdown, characterized by chaotic, high-frequency fluctuations that significantly enhance momentum and heat transfer rates [5].

Figure 4 illustrates the complete process and the distinct stages involved in the laminar-to-turbulent transition.

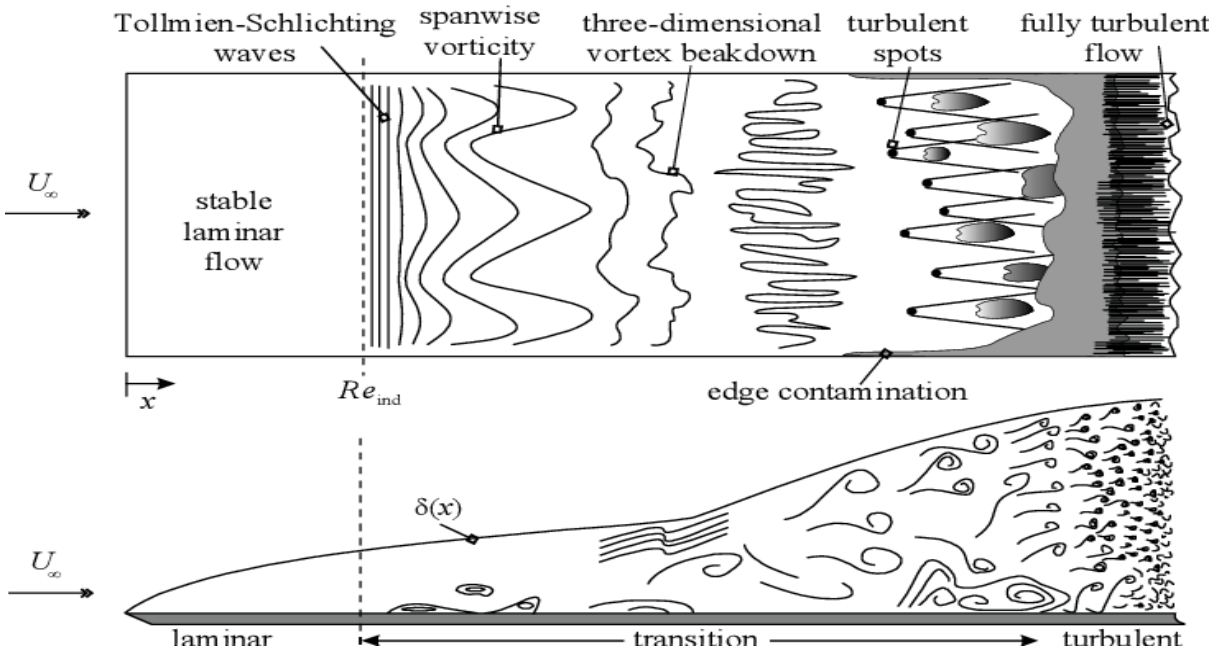

Figure 4 - laminar to turbulent transition: stages [39]

2.2 Effects of Various Factors on the Transition Process

The transition from laminar to turbulent flow is influenced by several key factors, among which the Reynolds number is one of the most critical. It serves as a measure of the relative importance of inertial forces to viscous forces in the flow. A higher Reynolds number typically leads to earlier transition, as it increases the likelihood of instability within the boundary layer [6].

Another important factor is the presence of an adverse pressure gradient, a condition where pressure increases in the direction of the flow. This gradient tends to destabilize the boundary layer by thickening it and promoting flow separation, thereby advancing the onset of turbulence. Similarly, surface roughness can introduce localized disturbances that trigger premature transition, especially when roughness elements exceed the critical height for laminar stability [7].

In many real-world environments, free-stream turbulence originating from upstream disturbances or environmental fluctuations is a dominant factor. FST interacts with the boundary layer and accelerates instability growth, particularly in bypass transition scenarios where traditional instability mechanisms (such as Tollmien-Schlichting waves) are bypassed altogether [8].

The stability of the boundary layer is also affected by flow geometry and rotational effects. For example, in rotating systems such as wind turbine blades, the interaction between crossflow instabilities and Kelvin–Helmholtz modes can either delay or promote transition, depending on the rotation rate and curvature of the surface [13].

2.2.1 Effect of Free-Stream Turbulence

The intensity and structure of free-stream turbulence (FST) play a crucial role in influencing the laminar-to-turbulent transition within boundary layers. Bienner et al. investigated this effect in both air and organic vapor flows using Large Eddy Simulation (LES). Their study demonstrated that an increase in FST intensity consistently advances the onset of transition, indicating that higher turbulence levels promote earlier development of turbulence in boundary layers for both fluid types.

Interestingly, the research also revealed a complex relationship between the integral length scale of turbulence (L_f) and the transition process. At a low turbulence intensity ($T_u = 2.5\%$) increasing L_f led to earlier transition. However, at a higher turbulence intensity ($T_u = 4\%$) a larger integral scale appeared to delay the transition. This behavior suggests that larger turbulent structures may increase the spacing between laminar streaks, thereby altering the growth and interaction of instabilities within the boundary layer [9].

In another study, Kumar et al. examined the impact of FST on boundary layer transition under an adverse pressure gradient using constant-temperature hotwire anemometry and electronically scanned pressure (ESP) measurements. Experiments were performed at two FST levels: 1.05% and 3.5%, while maintaining the same Reynolds number and pressure gradient

throughout. At the lower turbulence intensity of 1.05% , a laminar separation bubble was observed, indicating that the boundary layer remained stable enough for separation and subsequent natural transition. However, at the higher turbulence level of 3.5%, the flow behavior changed significantly. The laminar separation bubble was completely suppressed, suggesting that elevated FST destabilized the boundary layer, preventing the formation of stable laminar regions and leading to premature transition [10].

Von Ende Dotto et al [11] conducted Large-Eddy Simulations (LES) to study the transition mechanisms in a zero-pressure-gradient boundary layer developing over a flat plate, with varying free-stream turbulence intensities. Their findings revealed that at high free-stream turbulence levels, the transition occurs entirely through bypass mechanisms, characterized by the amplification of a continuous Orr–Sommerfeld (O–S) mode, which subsequently breaks down due to secondary instabilities. In contrast, under low turbulence conditions, both discrete and continuous O–S modes interact during the transition process. This interaction provides critical insight into the transitional behavior of boundary layers under different turbulence regimes and highlights the complexity of turbulence development under varying disturbance environments.

In another study, Borodulin et al [12] investigated the influence of distributed micro-sized roughness (MSR) elements on the transition from laminar to turbulent flow in a swept-wing boundary layer, with a specific focus on freestream turbulence effects. The results showed that, under optimal MSR configurations, the transition location could be significantly shifted downstream, effectively delaying turbulence onset. However, as the turbulence intensity increased, the transition moved upstream, indicating a reduction in the effectiveness of the MSR elements. This outcome suggests that the performance of passive roughness-based transition control strategies is highly sensitive to ambient turbulence levels.

2.2.2 Effects of Surface Roughness on Transition from Laminar to Turbulent

Surface roughness plays a significant role in destabilizing the boundary layer and can markedly affect the transition from laminar to turbulent flow. Wang et al [14] conducted a study to examine how randomly distributed surface roughness influences boundary layer stability. Their results showed that a roughness patch with a roughness Reynolds number (Re_{kk}) of 474 had a profound effect on transition. It generated streamwise streaks downstream of the rough region, which exhibited a stabilizing effect on Mack mode instabilities, but at the same time supported highly unstable shear-layer modes. The most amplified of these shear-layer modes primarily extracted energy from the spanwise velocity gradient, leading to nonlinear development into hairpin vortices. These vortices, concentrated around the strongest low-speed streaks, eventually propagated and contaminated the entire flow field, resulting in the onset of fully turbulent behavior.

In a 2024 study, Gokul et al [15] employed Direct Numerical Simulation (DNS) to analyze the influence of surface roughness on plane Couette flow (pCf), characterized by one rough stationary wall and one smooth moving wall. The investigation focused on two distinct roughness types: k-type and d-type, differentiated by their pitch separation (λ). For the k-type roughness (λ = 10k), laminar-turbulent bands were observed to stabilize at lower Reynolds numbers in the range Re ∈ [300, 325], marking a downward shift in the transitional Reynolds number range compared to smooth pCf, where transition typically occurs at Re ∈ [325, 400] .In contrast, d-type roughness (λ = 2k) caused a surprising upward shift in the transitional Reynolds number range to Re ∈ [350, 425]. This behavior was attributed to the d-type roughness's reduced capacity to shed vortices into the outer flow, thereby limiting its role in vorticity regeneration and delaying transition.

Ishita Jain et al [16] investigated the influence of surface roughness geometry on flow transition using well-resolved Large Eddy Simulations (LES). The study analyzed three different types of rough wall elements: triangular, square, and semi-circular. Each shape was found to significantly affect the underlying transition mechanisms within the boundary layer.

The triangular elements, characterized by sharp tips, were shown to promote transition primarily through the development of Kelvin–Helmholtz (K–H) instabilities in the shear layer. This result underscores the sensitivity of shear-layer dynamics to roughness geometry. In contrast, square roughness elements led to the formation of Λ-vortices, which play a key role in initiating the breakdown to turbulence. This indicates that the geometry of surface roughness directly influences the types of vortical structures that emerge during transition.

For semi-circular elements, the dominant mechanism was the generation of longitudinal streaks, highlighting yet another distinct pathway for transition driven by surface shape. Overall, the study illustrates that roughness geometry is a crucial factor in determining the nature and timing of boundary layer transition.

In another study, Borodulin et al [17] explored roughness-induced transition in a swept-wing boundary layer under the influence of freestream turbulence (FST). Using infrared thermography, they captured detailed observations of boundary layer behavior under various configurations. A key finding was a downstream shift in the transition location due to the implementation of micro-sized roughness (MSR) elements, indicating their effectiveness in delaying transition and enhancing boundary layer stability. The MSR elements were found to excite stationary vortices within the boundary layer. These vortices modified both the base flow and its stability characteristics, contributing significantly to the success of the transition control strategy.

S.M. Ananth et al [18] conducted a numerical investigation to study the impact of realistic roughness scales on the transition behavior of a laminar boundary layer. Their findings revealed that the onset of transition is highly sensitive to the scale and distribution of roughness features on the surface. The inclusion of finer roughness scales led to more complex flow behavior and significantly altered the transition process. Specifically, finer scales reduced the spacing between roughness elements, which constrained the lateral development of streaks within the boundary layer. This confinement resulted in weaker streamwise streaks, primarily due to the mutual sheltering effect of closely spaced roughness features. This effect was

especially pronounced at low Reynolds numbers (Re = 360). Moreover, the presence of fine-scale roughness introduced spanwise inhomogeneity in the flow across the transition region, causing variations in flow behavior along the width of the boundary layer and influencing the overall transition dynamics. Conversely, when finer roughness scales were filtered out, the study observed an earlier onset of transition. This was attributed to the formation of strong streaks generated by horseshoe vortices around more sparsely distributed roughness elements, which enhanced the instability and promoted earlier breakdown to turbulence.

2.2.3 Effects of Pressure Gradient on Laminar-to-Turbulent Transition

Pressure gradients have a profound influence on boundary layer development and play a critical role in the transition from laminar to turbulent flow. In particular, adverse pressure gradients (APGs) where pressure increases in the direction of the flow are known to destabilize boundary layers, leading to earlier transition, altered turbulence structures, and changes in separation and reattachment behavior.

Kumar et al [19] investigated the effects of APG on the transition of a laminar separation bubble (LSB) formed over a flat plate using electronically scanned pressure (ESP) sensors and a hotwire anemometer. Experiments were conducted at a Reynolds number of $Re = 2 * 10^5$ and a freestream turbulence intensity of 1.02%, with three different divergence angles ($\propto = 7^{\circ}, 9.5^{\circ}$ and 11.5°).

For the baseline case with $\alpha = 7^{\circ}$, the onset of separation was observed at $\frac{x}{L} = 0.39$, the transition point at $\frac{x}{L} = 0.449$, and flow reattachment at $\frac{x}{L} = 0.491$. As the adverse pressure gradient increased, all three points shifted upstream, indicating that stronger APGs cause earlier separation and transition. The length of the laminar separation bubble decreased with increasing APG, demonstrating that higher pressure gradients reduce the stability of the boundary layer. Moreover, the growth rate of velocity fluctuations increased with the severity of the pressure gradient, highlighting a higher susceptibility to transition under stronger APG conditions.

In another study, the combined effects of adverse pressure gradient and surface curvature were analyzed in the context of compressor duct flows. The results showed that curvature significantly influences the distribution of the pressure coefficient (Cp). On the outer wall, curvature led to a reduction in Cp from +0.19 to –0.6, indicating that approximately 75% of the surface was subjected to a favorable pressure gradient, which supports boundary layer stability and reduces drag. Conversely, the inner wall experienced an increase in Cp from –0.54 to +0.14, indicating the dominance of an adverse pressure gradient. This APG resulted in significant modifications to turbulence characteristics along the inner wall, increasing flow irregularity and boundary layer thickness. The thickening of the boundary layer in this region leads to higher skin friction drag and reduced flow efficiency, which can be detrimental in turbomachinery applications such as compressors [20].

As part of a joint research effort between the Japan Aerospace Exploration Agency (JAXA) and the National Aeronautics and Space Administration (NASA), the stability of boundary layer transition along the leeward symmetry plane of axisymmetric bodies at nonzero angles of incidence in supersonic flow was investigated. The study combined numerical simulations with experimental measurements to analyze boundary layer stability over five different body geometries, including the Sears–Haack body and several conical configurations. This integrated approach provided a comprehensive understanding of transition mechanisms under supersonic conditions [21].

One of the key findings was the strong influence of axial pressure gradients on boundary layer behavior. The study demonstrated that adverse axial pressure gradients consistently led to earlier transition within the boundary layer. This result was supported by both the numerical and experimental data, emphasizing the central role of pressure gradients in dictating transition onset in compressible flows. Furthermore, the destabilizing effects of these pressure gradients were attributed to three-dimensional flow dynamics. In particular, under adverse axial pressure conditions, a buildup of secondary flow along the leeward symmetry plane was observed.

This secondary flow mechanism intensified the instability of the boundary layer, thereby accelerating the transition to turbulence [21].

2.3 Flow Control

Flow control in fluid mechanics refers to the application of techniques and systems designed to regulate the behavior of fluid motion, including parameters such as velocity, pressure, and flow rate. Effective flow control is critical for optimizing performance across a wide range of engineering systems, such as hydraulic actuators, wind turbines, and aerospace structures.

Flow control strategies can be broadly categorized into passive and active methods:

1. **Passive flow control** involves modifications that influence the flow without requiring external energy input. These methods are typically implemented through structural changes or geometric modifications, for example, altering the shape of a surface or channel. Passive techniques are widely used for reducing flow resistance, delaying separation, and minimizing drag, making them particularly valuable in aerospace and automotive applications. Their simplicity and energy independence make them attractive, although their adaptability to changing flow conditions is limited.
2. **Active flow control (AFC)**, on the other hand, refers to techniques that require energy input to dynamically manipulate the flow field. Unlike passive methods, AFC systems can be tuned in real time to respond to changing flow conditions. Common mechanisms include synthetic jets, oscillatory blowing and suction, plasma actuators and localized heating or cooling. AFC techniques are particularly effective for applications requiring precise control over flow separation, transition, and turbulence levels, offering potential benefits such as drag reduction, lift enhancement, and noise suppression.

In this section, we will examine various active flow control methods used in engineering applications. We will discuss their underlying physical principles, advantages, and limitations to provide a comprehensive understanding of the role and potential of AFC in advanced flow management systems.

2.3.1 Boundary Layer Suction

Boundary Layer Suction (BLS) is an active flow control technique employed to improve aerodynamic performance by manipulating the boundary layer over surfaces such as airfoils and hydrofoils. The method involves extracting low-energy fluid near the surface, which stabilizes the boundary layer and delays flow separation. Suction removes low-momentum fluid near the surface, reducing boundary layer thickness and preventing separation at high angles of attack (AoA). This results in an increase in the net lifting force, thus enhancing lift generation [41].

The effectiveness of BLS is highly dependent on several parameters, including the location of suction, the diameter of the suction ports, and the suction angle. These factors can significantly influence the local flow characteristics and overall aerodynamic behavior. Figure 5 illustrates a typical implementation of the boundary layer suction technique on a surface.

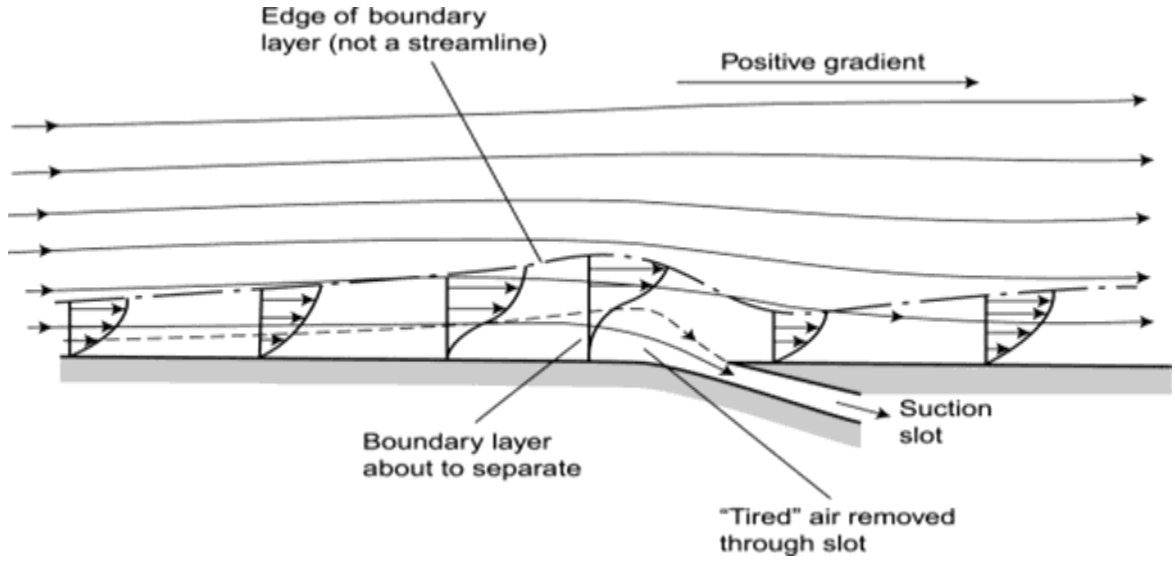

Figure 5 - BLS Method Implementation [40]

Experimental and numerical studies, particularly on the NACA 0012 airfoil, have demonstrated that Boundary Layer Suction, a form of Laminar Flow Control can suppress both boundary layer transition and flow separation. Specifically, the use of two-zone suction has been shown to improve lift and reduce drag by weakening vortex shedding mechanisms. Suction applied near the leading edge is especially effective in delaying separation, while suction closer to the trailing edge contributes to suppressing vortex formation and improving flow uniformity [42].

In hydrofoil applications, suction increases the velocity gradients in the boundary layer, thereby delaying the onset of transition and reducing the frequency of vortex shedding. This leads to an improvement in the lift-to-drag ratio, contributing to more efficient hydrodynamic performance.

BLS also plays a critical role in Hybrid Laminar Flow Control (HLFC) systems, which aim to maintain laminar flow over extended portions of the airfoil surface. This contributes to greater aerodynamic efficiency, especially in high-performance applications. Both wind tunnel experiments and computational simulations have validated the ability of BLS to delay laminar separation bubbles and enhance overall aerodynamic performance.

However, despite its advantages, boundary layer suction can introduce practical challenges. These include the need for precise control over suction parameters to avoid undesirable effects such as loss of total pressure recovery or degraded flow uniformity, particularly in complex geometries like S-shaped inlets or multi-element airfoils.

Hader et al [22] investigated the delay of transition onset in hypersonic flows (Mach 6) using Direct Numerical Simulation (DNS). To mimic natural transition processes typically observed in wind tunnel experiments, random disturbances were introduced at the inflow. Both the simulations and experimental results revealed the formation of streamwise “hot” streaks on the surface of a flared cone. These streaks were generated through the nonlinear interaction between an axisymmetric second-mode wave and a pair of oblique waves, a mechanism known as fundamental resonance. The

study proposed a flow control strategy based on the application of steady blowing and suction strips. This method was found to significantly delay the formation of hot streaks, thereby mitigating the adverse effects associated with nonlinear transition stages, such as elevated wall-pressure fluctuations.

Further analysis demonstrated that steady local blowing/suction effectively suppresses hypersonic boundary layer instabilities by broadening the frequency bandwidth of disturbance attenuation, inducing acoustic transport, and dampening dominant instability modes. A relatively small mass flux of blowing/suction aligns the critical frequency of the instability with the synchronization frequency, indicating a strong coupling between the control method and the inherent instability modes. As the mass flux increases, the bandwidth for disturbance suppression expands, enhancing the effectiveness of the control strategy. These findings underscore the potential of blowing and suction techniques in delaying transition in hypersonic flows, which is of critical importance in high-speed aerospace applications where maintaining boundary layer stability directly influences thermal protection, drag, and vehicle performance [23].

In 2024, Li causi et al performed a numerical investigation to evaluate the effectiveness of Boundary Layer Suction (BLS) as an active flow control method for transition delay over a flat plate. The study employed a custom-developed solver (BLES) to integrate the boundary layer equations, introducing suction through wall boundary conditions. Validation of the numerical framework was performed by comparison with Blasius and OpenFOAM solutions. Linear Stability Theory (LST) was applied to assess local and modal stability using the Companion Matrix Method for solving the Orr–Sommerfeld equation, and transition was modeled using the e^N method.

A Bayesian optimization approach was used to identify optimal suction configurations, focusing on suction velocity and region boundaries to maximize transition delay. Over 1600 combinations of parameters were evaluated. Results revealed that the optimal suction region typically extends between 8% and 20% of the plate length, with both location and strength of suction significantly influencing the transition position. A predictive model

was proposed to correlate suction configuration with transition behavior, achieving an agreement within 1% accuracy when validated against the numerical framework.

The study also showed that the envelope slope downstream of the suction region depends primarily on the suction mass flow and not on the precise suction location. Drag reduction analyses based on empirical correlations indicated that properly tuned suction could achieve up to 55% reduction compared to natural transition cases. Further extensions of the framework to non-uniform suction profiles, Falkner–Skan flows, and RANS simulations with the γ–Reθ model were proposed for future development [24].

2.3.2 Plasma Actuators

A plasma actuator, particularly the Dielectric Barrier Discharge (DBD) plasma actuator, is an active flow control device that manipulates airflow through the generation of plasma. It consists of two asymmetric electrodes separated by a dielectric layer. When a high-voltage alternating current (AC) is applied across the electrodes, the air in the vicinity of the exposed electrode becomes ionized, producing plasma. This ionized region generates a body force that interacts with the surrounding neutral air, inducing a secondary flow along the surface.

The working principle of a DBD plasma actuator is rooted in electrohydrodynamic (EHD) forcing. Upon applying a high-voltage AC signal, the electric field ionizes the air near the exposed electrode, creating charged particles (ions and electrons). These charged particles experience a force in the presence of the electric field and subsequently transfer momentum to neutral air molecules through collisions. This momentum transfer produces a tangential airflow along the actuator surface even in the absence of external flow.

The velocity of this induced flow can reach several meters per second, depending on parameters such as the applied voltage, frequency, electrode configuration, and ambient conditions. This makes plasma actuators particularly attractive for applications involving boundary layer control,

separation delay, and noise reduction. Figure 6 illustrates the basic working principle of a DBD plasma actuator installed on a surface.

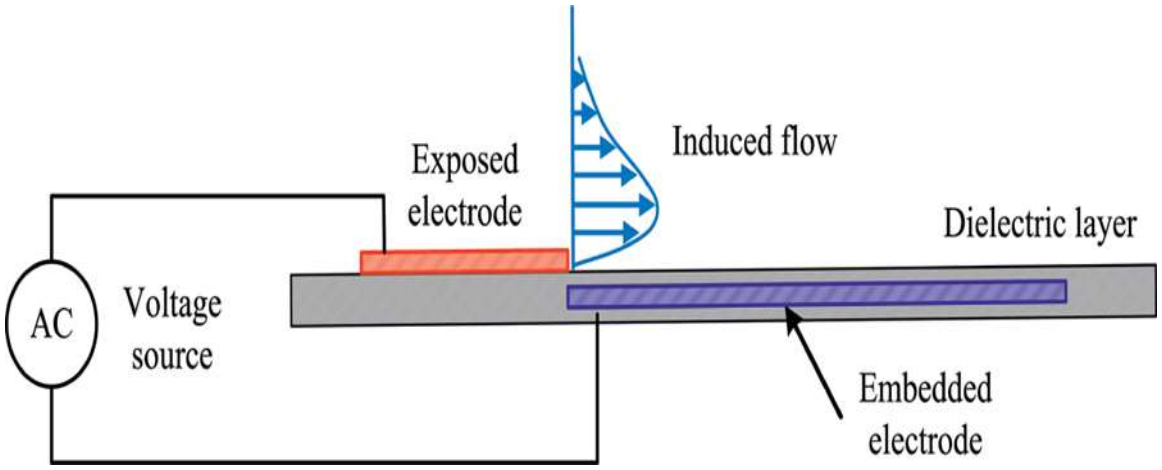

Figure 6 - Schematic of Plasma Actuator working principle [38]

Plasma actuators have demonstrated significant potential in modifying the aerodynamic characteristics of various surfaces such as aircraft wings, wind turbine blades, and other engineering structures without requiring any mechanical moving parts. This is achieved through localized plasma discharges that interact with the surrounding airflow, enabling enhanced boundary layer control and flow separation suppression.

Plasma vortex generators (PVGs) have shown to create controlled vortical structures that manipulate the airflow near the surface. These vortices contribute to drag reduction and lift enhancement, making plasma-based actuation attractive for a wide range of applications in the automotive, marine, and aerospace sectors. The ability to achieve such flow control non-intrusively offers a promising pathway for improving the aerodynamic efficiency of high-performance systems [25].

In a notable experimental study, Yurchenko et al [26] investigated the effectiveness of plasma actuators for flow control using a 12.5% supercritical airfoil model tested in a wind tunnel. The airfoil was fitted with a spanwise array of pulsating high-voltage plasma discharges, functioning

as an active flow control system. The results revealed a significant improvement in aerodynamic performance:

a. The maximum lift coefficient (CLmax) increased by up to 10%, indicating enhanced lift generation.
b. The stall angle of attack increased by 1.5° to 3.5°, enabling the airfoil to operate at higher angles before experiencing flow separation and stall.
c. A drag reduction of up to 7% was also observed, contributing to improved fuel efficiency and overall aerodynamic performance.

Experimental studies investigating boundary layer transition control using plasma actuators have consistently demonstrated the effectiveness of this technology in delaying transition and reducing drag. In one study, a parallel Dielectric Barrier Discharge (DBD) plasma exciter was designed and tested to assess its performance. The Particle Image Velocimetry (PIV) technique was employed to visualize and quantify the spatial flow field distributions generated by both single-stage and three-stage actuators. The actuator was applied to a super-zero-boundary airfoil, successfully controlling flow separation.

To further analyze the effect of the plasma actuator on transition dynamics, the study also utilized the oil droplet interferometric method. Results showed that increasing the discharge voltage of the actuator led to a noticeable reduction in wall drag and a more effective delay in the boundary layer transition. These findings suggest that the jet-like effect produced by the actuator plays a crucial role in stabilizing the near-wall flow and enhancing overall flow behavior [27].

In 2017, Serpieri et al [43] investigated the selective forcing of cross-flow instability modes on a 45° swept wing at Re = $2.17 * 10^6$ using spanwise-modulated dielectric barrier discharge (DBD) plasma actuators placed near the leading edge. The study adopted an active implementation of the discrete roughness elements/upstream flow deformation (DRE/UFD) strategy for laminar flow control (LFC), previously explored by Saric et al.

(1998), Malik et al. (1999), and Wassermann & Kloker (2002). Custom-designed alternating current plasma actuators were developed and experimentally characterized to force monochromatic stationary cross-flow modes at various spanwise wavelengths. Infrared thermography and time-resolved particle image velocimetry (TR-PIV) were used to capture thermal and velocity field responses, respectively. Results showed that the actuators introduced steady and unsteady fluctuations in the boundary layer, amplifying at frequencies significantly lower than the forcing frequency. In particular, sub-critical mode forcing (shorter wavelength than the naturally selected one) led to a reduction in the amplification of primary vortices. The measured actuator body force was then coupled with a laminar boundary layer solution and linear stability theory to evaluate the influence of steady forcing on flow stability. This simplified numerical framework provided fast and cost-efficient estimates of the impact of body force magnitude and direction on boundary layer receptivity and transition.

In a more recent study conducted in 2024, Zhang et al [28] examined the transition flow control on the suction surface of a highly loaded compressor cascade using plasma actuators. The study demonstrated that plasma actuation could effectively delay the laminar-to-turbulent transition, thereby reducing flow losses and improving aerodynamic efficiency within the cascade.

A key result of this research was the finding that actuator placement is critical to performance. The most effective location was identified to be upstream of the separation bubble, which led to a 6.32% reduction in total pressure loss and a 2.5% increase in static pressure rise. These improvements underscore the actuator's capability to enhance compressor cascade performance.

However, the study also highlighted certain complex flow interactions, particularly in the end-wall region. The plasma actuator was observed to increase the accumulation of low-energy fluid in the corner region, which in turn caused a slight increase in shear losses between the midspan boundary layer and the corner flow. This suggests that while the actuators offer clear aerodynamic benefits, their implementation must be carefully managed to avoid introducing secondary losses in complex geometries.

Xiao et al [29] investigated bypass transition in flow over a flat plate induced by a pair of Dielectric Barrier Discharge (DBD) plasma actuators mounted on the surface and aligned in the streamwise direction. The actuators produced a distinct velocity streak pattern, with a central high-speed streak flanked by two low-speed streaks. This streak formation plays a critical role in promoting the laminar-to-turbulent transition. The study found that increasing the length of the plasma actuators enhanced momentum injection into the boundary layer, ultimately leading to the formation of a turbulent wedge at a nearly constant streamwise location. This indicates a strong relationship between actuator length and transition onset.

The spanwise configuration of the actuators also significantly influenced the transition mechanism. A wide layout (larger spacing between actuators) led to the simultaneous destabilization of the low-speed streaks through an inclined varicose-like mode, resulting in a symmetric perturbation pattern. In contrast, a narrow layout (closely spaced actuators) intensified the mean shear near the centerline, causing the high-speed streak to become unstable first, which led to an asymmetric disturbance pattern.

In a related 2021 study, Kang et al [30] conducted numerical simulations to explore the control of transition-inducing stationary crossflow vortices using distributed plasma actuation. The control strategy involved generating sub-dominant “killer” modes aimed at suppressing the dominant transition-causing disturbances. Using a linearized Navier-Stokes (LNS) solver, the simulations showed good agreement with experimental data from the TsAGI T124 wind tunnel.

The numerical results predicted that introducing killer modes would delay the transition to turbulence. However, the experimental findings contradicted this prediction, revealing an unexpected advancement of the transition. This discrepancy was attributed to unsteady effects induced by the plasma actuators, which inadvertently excited traveling crossflow disturbances. These disturbances interacted with the target stationary modes, undermining the intended stabilization.

The LNS simulations were effective in modeling the generation of killer modes, and their amplitudes were used as input for nonlinear parabolized

stability equation (PSE) analysis. While the PSE analysis supported the theoretical delay in transition, the experiments emphasized a practical challenge: the unsteady nature of plasma actuation can interfere with the desired control mechanism, ultimately accelerating transition instead of suppressing it.

In another study, Rizzetta et al [31] investigated the effect of compressibility on plasma-based transition control for a wing with leading-edge excrescence. The research utilized numerical simulations to explore how compressibility effects influence the performance of Dielectric Barrier Discharge (DBD) plasma actuators in delaying the laminar-to-turbulent transition. This delay is especially important because premature transition often leads to increased drag and a decrease in energy efficiency.

The study examined various Mach numbers, including values extending into the transonic regime. It was observed that the effectiveness of the plasma actuators improved with increasing Mach number, indicating a positive correlation between compressibility effects and actuator performance. At higher speeds, the plasma actuator not only delayed transition but also mitigated turbulence, contributing to smoother airflow over the wing surface.

These findings have significant implications for aerodynamic efficiency, particularly in high-speed applications such as reconnaissance missions, where maintaining laminar flow reduces drag and enhances fuel economy. The research concludes that plasma-based flow control, coupled with compressibility advantages, can serve as an effective strategy to optimize aerodynamic performance.

In a related 2017 study, Dorr et al [32] explored the role of upstream flow deformation (UFD) in controlling transition using plasma actuators, particularly in scenarios involving crossflow induced by unsteady vortical disturbances. The investigation focused on conditions of low free-stream turbulence, where surface roughness can trigger premature transition.

The study demonstrated that UFD generated by plasma actuators is highly effective in delaying transition from laminar to turbulent flow. By manipulating the upstream flow characteristics, the technique offers a

promising method to influence boundary layer stability and extend the laminar flow regime over surfaces susceptible to early transition.

The results also revealed that UFD can significantly modify crossflow dynamics, especially in the presence of unsteady disturbances. This implies that upstream flow manipulation can counteract the destabilizing effects of such disturbances, thus offering a non-intrusive and adaptive strategy for managing transition in complex flow environments.

Chapter 3: Governing equations and Problem setup

3.1 Governing Equations

The study of active flow control using Dielectric Barrier Discharge (DBD) plasma actuators necessitates a rigorous theoretical foundation in both fluid dynamics and electric body force. The interaction between the plasma-induced body force and the airflow is governed by a system of fundamental equations derived from the conservation laws of mass, momentum, and energy. These equations collectively referred to as the Navier–Stokes equations describe the motion and evolution of fluid flows under various internal and external influences.

In the specific context of DBD plasma actuators, an additional body force term is incorporated into the momentum equation to represent the effect of plasma-induced acceleration near the wall. This force arises from electrostatic interactions, wherein charged particles generated by the plasma impart momentum to the surrounding neutral air molecules through collision and momentum transfer.

A detailed understanding of these governing equations is essential for accurately modeling the influence of plasma actuation on boundary layer development, transition mechanisms, and aerodynamic performance. This section presents a comprehensive derivation of the relevant governing equations, elaborates on the role of plasma-induced body forces, and discusses the numerical implementation strategies adopted in Computational Fluid Dynamics (CFD) simulations, particularly those conducted using ANSYS Fluent.

3.1.1 Conservation of Mass

The conservation of mass is a fundamental principle in fluid mechanics, asserting that mass cannot be created or destroyed within a control volume. This principle is mathematically formulated through the continuity equation,

which ensures that the rate of mass entering a control volume equals the rate of mass exiting, adjusted for any accumulation of mass within the volume.

In its differential form, the general continuity equation for a compressible flow is expressed as:

$$\frac{\partial \rho}{\partial t} + \ div\left(\rho \vec{V}\right) = 0 \qquad (3\text{-}1)$$

Where (.) represents dot product. This equation serves as the foundation for modeling fluid behavior in both steady and unsteady flows and is essential in ensuring mass conservation in Computational Fluid Dynamics (CFD) simulations.

3.1.2 Conservation of Momentum

The Navier-Stokes equation embodies the principle of momentum conservation in fluid dynamics. It describes how the momentum of fluid particles is preserved as they move and interact with external and internal forces. These equations lead to three additional expressions that help determine six essential field variables required to fully describe a fluid system, namely, three velocity components, pressure, density, and temperature. The principle of momentum conservation asserts that the total momentum within a fluid system remains constant unless influenced by external forces. This is a direct application of Newton's Second Law to fluid flow.

$$\frac{\partial}{\partial t}(\rho V) + div(\rho VV) = \ -\nabla \mathrm{P} + \ div(\vec{\tau}) + \ \rho \mathrm{g} \qquad (3\text{-}2)$$

In this formulation P denotes the pressure, τ is the viscous stress tensor acting on a fluid element, and g represents gravitational acceleration. The equation indicates that the rate of change of momentum is influenced by the convective term $div(\rho VV)$, which accounts for the transport of momentum by the fluid's motion; by the pressure gradient term $-\nabla \mathrm{P}$, which represents forces arising from spatial pressure variations in the flow field; by the viscous term $div(\vec{\tau})$caused by internal friction in fluid elements due to viscosity and by external body forces like gravity or a source term.

3.1.3 Turbulence

Turbulence is a chaotic and irregular state of fluid motion, characterized by swirling vortices (eddies), rapid fluctuations in velocity and pressure, and elevated energy dissipation. It typically arises when the Reynolds number is sufficiently high, indicating that inertial forces dominate over viscous forces. This transition from laminar to turbulent flow can occur even in the absence of external disturbances, as first demonstrated by Osborne Reynolds in 1883 through his classical pipe flow experiments [44].

The transition to turbulence is influenced by several factors, most notably fluid viscosity and the Reynolds number, which quantifies the ratio of inertial to viscous forces. Accurate modeling of turbulence is critical in fluid dynamics, as turbulent flows are common in numerous engineering applications. The complex nature of turbulence marked by chaotic, multi-scale motion requires advanced modeling techniques to accurately represent its behavior.

Turbulence modeling plays a vital role in optimizing designs across fields such as aerospace, chemical processing, and energy systems. However, modeling turbulent flows introduces the closure problem: the Navier-Stokes equations contain more unknowns than equations when applied to turbulent regimes. This discrepancy necessitates the use of turbulence models that relate these unknowns to the resolved scales of motion.

Among the most widely used approaches in engineering are Reynolds-Averaged Navier-Stokes (RANS) models. These models decompose the instantaneous velocity field into a mean component and a fluctuating

component and then apply time-averaging to the governing equations. This process results in additional terms known as Reynolds stresses, which must be modeled to achieve closure of the equations.

To derive the Reynolds stress terms, we begin by decomposing the velocity field into:

$$U = \overline{U} + \acute{u} \tag{3-3}$$

In this formulation, $\overline{U}$ represents the mean time-averaged velocity, while $\acute{U}$ denotes the fluctuating component of velocity at each point in the flow field. Similarly, the pressure field is decomposed into time-averaged and fluctuating components. By substituting these decomposed terms into the Navier-Stokes equations and recognizing that the time average of fluctuations is zero, we obtain the Reynolds-Averaged Navier-Stokes (RANS) equations.

$$\frac{\partial \overline{U}_i}{\partial t} + \overline{U}_j \frac{\partial \overline{U}_i}{\partial x_j} = -\frac{1}{\rho}\frac{\partial \bar{P}}{\partial x_i} + v \frac{\partial^2 \overline{U}_i}{\partial x_j \partial x_j} - \frac{\partial \overline{\acute{U}_\iota \acute{U}_J}}{\partial x_j} \tag{3-4}$$

The term $\overline{\acute{U}_\iota \acute{U}_j}$ is known as the Reynolds stress tensor, which represents the transport of momentum due to turbulence. Unlike molecular viscosity, which is directly proportional to velocity gradients, Reynolds' stresses originate from turbulent fluctuations and must be modeled separately. The RANS equations introduce six additional unknowns corresponding to the components of the Reynolds stress tensor but do not provide new equations to solve them. This discrepancy is known as the closure problem of turbulence. To resolve this, turbulence models are employed to approximate the Reynolds stresses. In this thesis, the Shear Stress Transport $k - \omega\ SST$ turbulence model is used to solve the Navier-Stokes equations within the CFD simulations.

3.1.4 $k-\omega$ SST Turbulence Model

The $k-\omega\ SST$ turbulence model is a widely adopted two-equation eddy-viscosity model formulated within the RANS framework. Developed by Menter [45] in 1994, the model effectively combines the advantages of the $k-\varepsilon$ and $k-\omega$ models to accurately capture turbulent flow behavior, especially in scenarios involving adverse pressure gradients and flow separation phenomena frequently encountered in engineering applications.

The $k-\omega\ SST$ model solves two transport equations: one for the turbulent kinetic energy and the other for the specific dissipation rate. These equations are blended using a carefully designed transition function to utilize the high accuracy of the $k-\omega$ formulation in the near-wall region and the robustness of the $k-\varepsilon$ model in free-shear flows. The blending function enables a smooth and consistent transition between the two regions, ensuring improved predictive capability across a wide range of flow conditions.

The transport equation for turbulent kinetic energy (k) is presented in Equation (3-5).

$$\frac{\partial(\rho k)}{\partial t}+\frac{\partial(\rho u_j k)}{\partial x_j}=P_K\ -\ \beta*\ \rho k\omega+\frac{\partial}{\partial x_j}\left[(\mu+\ \sigma_k\mu_t)\frac{\partial k}{\partial x_j}\right] \tag{3-5}$$

In which P_K is the production rate of K, σ_k and β are model coefficients and μ_t is eddy viscosity. For the transport of the specific dissipation rate ω, the following equation is used.

$$\frac{\partial(\rho\omega)}{\partial t} + \frac{\partial(\rho u_j \omega)}{\partial x_j} = \alpha\frac{\rho}{2} S^2 - \beta\rho\omega^2 + \frac{\partial}{\partial x_j}\left[(\mu + \sigma_\omega \mu_t)\frac{\partial\omega}{\partial x_j}\right] + 2(1-F_1)\rho\sigma_{\omega 2}\frac{1}{\omega}\frac{\partial k}{\partial x_j}\frac{\partial\omega}{\partial x_j} \quad (3\text{-}6)$$

In which S is strain rate magnitude which is defined as equation 3-7.

$$S = \sqrt{2S_{ij}S_{ij}} \quad (3\text{-}7)$$

F_1 is blending function which activates k-ω near walls and k-ε in freestreams. The advantages of this model includes Accuracy Near Walls: Resolves low-Reynolds-number effects without damping functions, Separation Prediction: Superior performance in adverse pressure gradients due to eddy viscosity limiter, Blended Formulation: Seamlessly transitions between k-ω (wall) and k-ε (free stream) models and limitations include isotropic turbulence assumption: Fails in strongly anisotropic flows (e.g., swirling flows), RANS limitations: Cannot resolve unsteady turbulence structures directly (unlike LES/DNS). The k-ω SST model balances accuracy and computational efficiency for industrial flows with separation and adverse pressure gradients. Its hybrid formulation makes it a versatile choice for complex boundary layer simulations, though users must carefully define boundary conditions and recognize its RANS-based limitations.

Prior to the γ-Reθ model, RANS turbulence models (e.g., k-ε, k-ω SST) assumed fully turbulent flow, leading to inaccuracies in transitional regions. Transition prediction traditionally relied on empirical correlations (e.g., Michel's method), which link transition onset to momentum thickness Reynolds numbers but lack generality and Integral boundary layer methods,

which solve simplified equations but struggle with complex geometries and 3D flows. These approaches were limited to simple configurations and required prior knowledge of transition locations [46]. The γ-Reθ model was developed by Langtry and Menter (2009) [46] to integrate transition prediction directly into RANS solvers. Key motivations included: Eliminating dependency on non-local integral parameters, capturing multiple transition mechanisms (natural, bypass, separation-induced) in a single framework, ensuring compatibility with the widely used k-ω SST turbulence model. The model leverages experimental correlations from the STAN7 database, a compilation of transition data for airfoils and flat plates under varying pressure gradients and turbulence intensities. Computational formulation lies in the definition of two parameters. Intermittency quantifies the temporal-spatial presence of turbulence in a boundary layer $\gamma = 0$ for fully laminar flow, $\gamma = 1$ for fully turbulent flow and the quantities between 0 and 1 for transitional flow. The γ-Reθ model solves a transport equation for γ dynamically activating turbulence production during transition.

The accuracy of γ–Reθ transition model has previously been proven in the literature by many researchers. Gang [33] Performed a study to investigate transitional flow behavior based on γ–Reθ model. In order to predict the boundary layer transition automatically in viscous flow simulation, Gamma Re-theta transition model is implemented in a hybrid unstructured RANS flow solver which was originally developed by the authors and named HUNS3D. The model was validated through simulations of free transitional flows around various aerodynamic configurations. The computed results from the simulations were compared with corresponding experimental data. The comparisons demonstrated that the model accurately predicts the natural transition of the boundary layer and the transition induced by separation. This accuracy is crucial for realistic flow simulations in engineering applications. In 2011 The γ–Reθ transition model was validated using numerical simulations in the TRIP software developed by the China Aerodynamics Research and Development Center [34]. The results showed that the transition locations for both natural and separated transitions aligned well with experimental data, confirming the model's accuracy in predicting flow behavior. The study examined the flow over various low-

speed airfoils, including S809, NLR7301, and 30P30N. The dynamic characteristics of these airfoils were analyzed, demonstrating that the model could effectively capture the transition phenomena occurring in these specific configurations [34].

With these validations in mind, we will provide the equations for this model, and we will use it in our simulation as the main transition model to capture these effects in the flow. Equations include intermittency and transport equation for transition momentum thickness Reynolds number.

$$\frac{\partial(\rho\gamma)}{\partial t} + \frac{\partial(\rho U_j \gamma)}{\partial x_j} = P_\gamma - E_\gamma + \frac{\partial}{\partial x_j}[(\mu + \frac{\mu_t}{\sigma_y})\frac{\partial \gamma}{\partial x_j}] \quad (3\text{-}8)$$

In equation 3-8, P_γ is the production term. The equation for product terms is as follows.

$$P_\gamma = F_{length} * \rho S * \gamma^{0.5}(1-\gamma) \quad (3\text{-}9)$$

Where S is strain rate magnitude, and F_{length} is an empirical correlation controlling the transition length. Also, for destruction we have:

$$E_\gamma = C_{a2} * \rho\Omega * \gamma * F_{turb} \quad \text{for } \gamma \geq 1 \quad (3\text{-}10)$$

Where Ω is vorticity magnitude, and F_{turb} is a blending function. The transport equation for transition momentum thickness Reynolds number allows non-local effects by transporting the transition onset criterion:

$$\frac{\partial(\rho\widetilde{Re}_{\theta t})}{\partial t} + \frac{\partial(\rho U_j\widetilde{Re}_{\theta t})}{\partial x_j} = P_{\theta t} + \frac{\partial}{\partial x_j}[\sigma_{\theta t}(\mu + \mu_t)\frac{\partial\widetilde{Re}_{\theta t}}{\partial x_j}] \quad (3\text{-}11)$$

Where $P_{\theta t}$ is source term.

$$P_{\theta t} = c_{\theta t}\frac{\rho}{t}(Re_{\theta t} - \widetilde{Re}_{\theta t}) \quad (3\text{-}12)$$

Where t is a timescale. Typically, $Re_{\theta t}$ is computed from experimental correlations based on freestream turbulence intensity and pressure gradient.

3.2 Shyy Body Force Model for DBD Plasma Actuators

The Shyy model, developed by Shyy et al [38] offers a simplified and computationally efficient approach for modeling the body force induced by DBD plasma actuators. Due to its ease of implementation and relatively low computational cost, this model is particularly well-suited for numerical simulations involving active flow control in aerodynamic applications.

In this model, the electric field generated by the DBD actuator is idealized using linear assumptions, as illustrated in Figure 7. In a typical DBD configuration, two asymmetric electrodes are used: one exposed to the air and the other embedded beneath a dielectric layer. When an AC voltage applied across the electrodes exceeds the dielectric breakdown strength of air, ionization occurs near the exposed electrode, resulting in the formation

of plasma. The charged particles within this plasma region impart momentum to neutral air molecules through electrostatic interactions, generating a body force that accelerates the airflow along the surface.

The Shyy model simplifies this complex interaction by assuming that the electric field intensity decreases linearly with distance from the exposed electrode. The spatial variation of the electric field is mathematically defined as follows:

$$\overrightarrow{E(x,y)} = E_0 - k_1 x - k_2 y \tag{3-13}$$

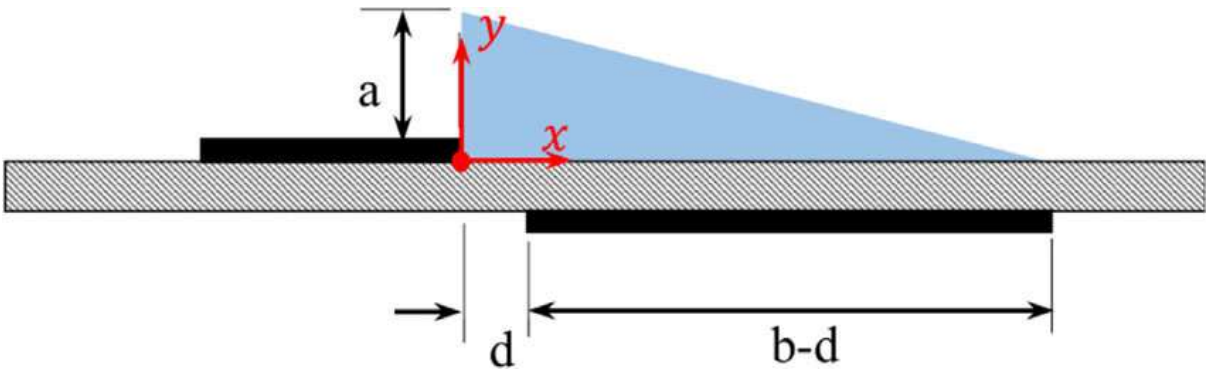

Figure 7 - Body Force distribution in shyy model [38]

Where $E_0 = \frac{V}{d}$ represents the maximum electric field strength determined by the applied voltage V and the electrode gap d. the constants k_1 and k_2 describe the gradients of the electric field in the x and y directions, respectively, and are computed using:

$$k_1 = \frac{E_0 - E_b}{b} \tag{3-14}$$

$$k_2 = \frac{E_0 - E_b}{a} \tag{3-15}$$

Here E_b is the dielectric breakdown strength of air (typically around 3 kV/cm), while a and b denote the height and width of the plasma region. The resultant body force per unit volume acting on the flow, $\overrightarrow{f_b}$, is then approximated as:

$$\overrightarrow{f_b} = \vec{E} * q_c * e * \alpha \quad (3\text{-}16)$$

where q_c is the net charge density (commonly assumed to be $1 * 10^{17} C/m^3$), e is the elementary charge (approximately $1.602 * 10^{-19} C$) and α is a correction factor introduced to accommodate empirical adjustments or model calibration. The resulting body force acts in the near-wall region, producing a jet-like flow along the surface. This momentum addition plays a crucial role in delaying or suppressing flow separation, especially over aerodynamic surfaces such as airfoils operating at high angles of attack.

One of the primary advantages of the Shyy model is its ease of integration with Computational Fluid Dynamics (CFD) solvers such as ANSYS Fluent. The plasma-induced body force can be incorporated directly into the Navier-Stokes equations via a User-Defined Function (UDF), eliminating the need to solve complex coupled electrostatic equations. This makes the Shyy model both computationally efficient and highly suitable for parametric investigations involving variations in plasma actuator configurations and input voltages.

Validation studies referenced in the original work indicate that the model provides reasonable agreement with experimental observations and more detailed simulations. Although it employs simplifying assumptions, most notably the linear distribution of the electric field, the Shyy model delivers sufficiently accurate predictions of flow control behavior for a wide range of practical engineering applications.

3.3 Finite Volume Method

In Computational Fluid Dynamics (CFD), the governing equations of fluid motion, namely the Navier–Stokes equations, are expressed in partial

differential form and must be transformed into a form suitable for numerical solution. This transformation process is known as discretization, and one of the most robust and widely adopted discretization techniques is the Finite Volume Method (FVM).

The FVM is particularly effective for solving both compressible and incompressible flows, and its primary advantage lies in its inherent conservation properties. Unlike other methods, such as the finite difference method, the FVM ensures that the conservation of mass, momentum, and energy is strictly enforced over each discrete control volume within the computational domain.

In the FVM, the flow domain is divided into a finite number of non-overlapping control volumes or cells, which can be structured (e.g., hexahedral or quadrilateral grids) or unstructured (e.g., triangular or tetrahedral meshes). The governing equations are then integrated over each control volume, and the divergence theorem is applied to convert volume integrals into surface integrals. This allows fluxes of conserved quantities—such as mass, momentum, or energy to be calculated across the surfaces of each control volume.

One of the major strengths of this method is its adaptability to complex geometries, making it well-suited for real-world engineering problems. It also facilitates the use of non-uniform grids, which enable mesh refinement in regions with high gradients (e.g., near walls or in boundary layers), improving solution accuracy without excessive computational cost.

The FVM also requires a closure model when applied to turbulent flows, as in the case of RANS simulations. This involves incorporating a turbulence model, such as the $k-\omega\ SST$ model used in this thesis to relate turbulent quantities to the mean flow.

To ensure a fully solvable system, the governing equations are typically closed using an equation of state, such as the ideal gas law, to relate pressure, density, and temperature. This closure is especially important in compressible flow simulations, where the interdependence of thermodynamic properties must be accurately resolved.

3.4 Problem Setup

The objective of this study is to investigate the effects of plasma actuators on fluid flow over a flat plate. A two-dimensional rectangular computational domain, measuring **4 meters in length** and **0.3 meters in height**, is selected, as illustrated in **Figure 8**. The choice of a two-dimensional setup significantly reduces computational cost while still providing reliable accuracy for flat plate boundary layer flows, where spanwise variations are minimal and can be reasonably neglected.

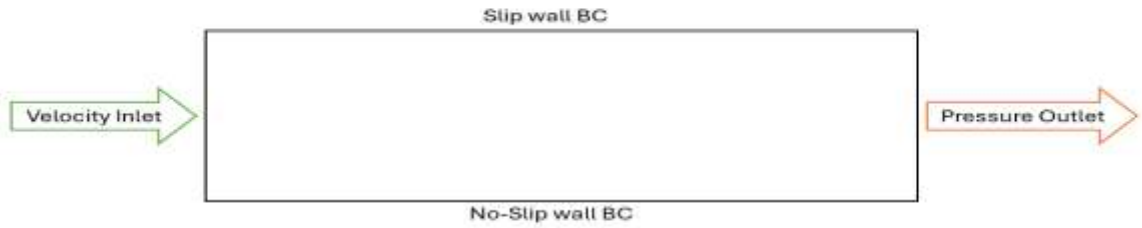

Figure 8 - Two-dimensional Flow domain

The left green arrow represents the inlet boundary, while the right red arrow indicates the outlet boundary. The bottom boundary is defined as a no-slip wall, and the top boundary is treated as a slip wall, as the effects of the boundary layer and flow control on the upper surface are intentionally excluded from the simulation.

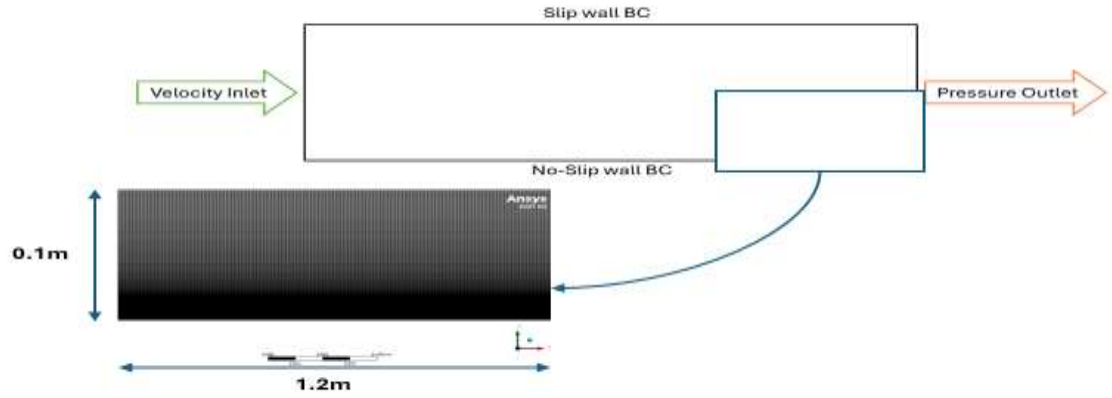

Figure 9 - Structured Two-dimensional Mesh

A structured two-dimensional rectangular mesh has been generated for this domain, with sufficiently refined elements in the near-wall region to accurately capture critical flow phenomena. Figure 9 presents a zoomed-in view of the mesh near the right corner of the flow domain for illustrative purposes. The mesh comprises approximately 480,000 elements, ensuring adequate resolution for simulating boundary layer development and the effects of plasma actuation. Cell growth ratio in the vicinity of wall and boundary layer was kept 1.05 to ensure adequate cell resolution in order to effectively capture laminar to turbulent transition location.

A major advantage of using a structured mesh lies in its computational efficiency. Due to the regular and predictable arrangement of cells, cell connectivity can be determined via indexing, which significantly reduces memory usage and enhances solver performance. Structured meshes also tend to offer greater accuracy and numerical stability in simulations involving simple geometries, particularly when the mesh is aligned with the flow direction.

The general simulation settings used in ANSYS Fluent are summarized in the table below. These parameters will remain constant throughout the study, unless stated otherwise in specific sections.

Pressure based steady state solver
Transition SST 4 equations turbulence model
Constant density air as the material
Inlet boundary type as velocity Inlet
Outlet Boundary type as Pressure outlet
Pressure-Velocity coupling scheme as coupled

Table 1 - General Settings for Simulations in ANSYS Fluent

3.4.1 User Defined Function (UDF)

ANSYS Fluent offers a wide range of built-in capabilities for simulating various fluid flow scenarios. However, many advanced or customized numerical models found in the literature are not natively included in the software. To implement such models, users can write a UDF in the C programming language, utilizing predefined macros and functions provided by Fluent.

In this study, a UDF is developed to incorporate the body force generated by the Shyy plasma actuator model as an additional source term in the Navier–Stokes equations. This integration is essential for accurately capturing the influence of plasma actuators on the fluid flow within targeted regions of the domain.

A distinguishing feature of this work, compared to previous studies, is the parameterization of key variables such as actuator voltage and location. Instead of assigning fixed constant values, these variables are defined as real parameters, enabling more flexible parametric studies and optimization routines to enhance flow control performance.

Implementing these parameters within the UDF requires the use of specific Fluent functions and additional configuration steps in the Graphical User Interface (GUI). The complete UDF code is provided in Appendix A for reference and further exploration.

Chapter 4: Results

This chapter presents the results of numerical simulations, beginning with the validation of the SST Transition (4-equation) model in ANSYS Fluent. The primary objective of this stage is to verify the accuracy of the transition prediction on a flat plate for various inlet velocities and turbulence intensity levels. This validation step is essential to ensure the credibility of subsequent simulations involving active flow control using plasma actuators.

4.1 Transition Modeling

To establish a reliable simulation baseline, several cases were modeled without active flow control, focusing solely on capturing the natural transition from laminar to turbulent flow over a flat plate. The simulation results were compared with experimental data reported by NASA [37], serving as a benchmark for model validation.

4.1.1 Case 1: Flat Plate Transition at 10.668 m/s, $T_u = \%1$

In the first case, the flat plate is subjected to an inlet velocity of 10.668 meters per second with a freestream turbulence intensity of 1%. The intermittency values at the inlet and outlet boundaries are set to 1, indicating a fully turbulent condition at the boundaries. The objective of this setup is to observe the transition behavior in the central region of the domain and verify whether the model accurately predicts the onset and development of turbulence under low turbulence intensity conditions.

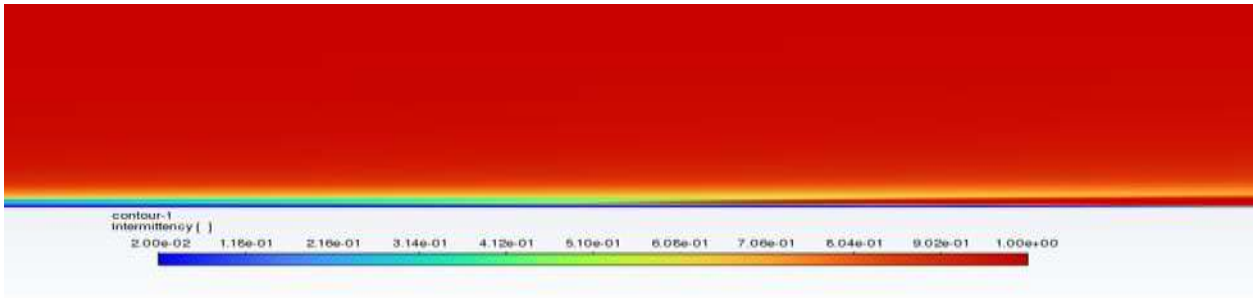

Figure 10 - Contour of Intermittency near transition location

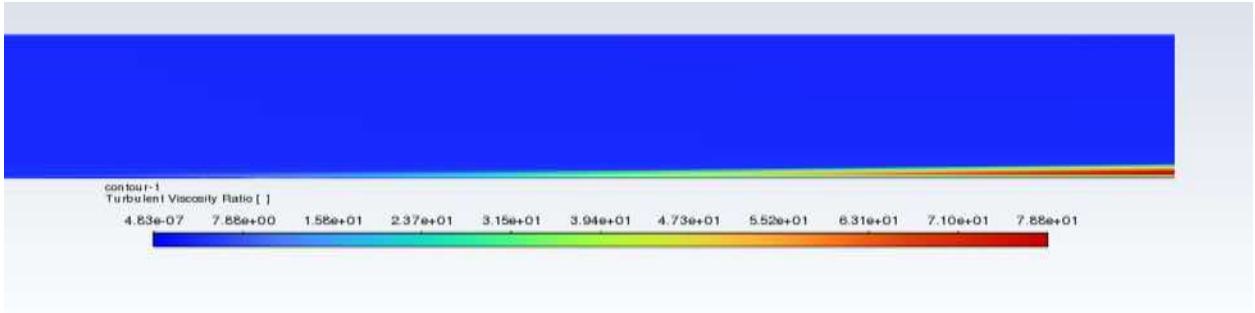

Figure 11 - Contour of Turbulent Viscosity ration near transition location

Figures 10 and 11 present the intermittency distribution and turbulent viscosity ratio near the transition region, which serve as reliable indicators for identifying the onset and development of laminar-to-turbulent transition. In the intermittency contour (Figure 10), the inlet boundary is prescribed with a value of 1, indicating fully turbulent flow. However, immediately downstream, within the boundary layer, the intermittency drops sharply, reflecting the laminar nature of the incoming flow. As the flow progresses along the streamwise direction, intermittency gradually increases, indicating a transitional regime, until it eventually approaches unity once more, corresponding to fully developed turbulence. The region where intermittency increases from near-zero to unity effectively marks the transition zone.

A similar trend is observed in the turbulent viscosity ratio (Figure 11), which represents the ratio of eddy viscosity to molecular viscosity. In laminar flow, this ratio remains close to zero due to negligible turbulence production. As the flow transitions, spatial fluctuations in this parameter emerge, shown by streaks or patches of elevated values within the boundary layer. When these structures become thicker and more uniform, the flow can be considered fully turbulent. Thus, the increase and stabilization of turbulent viscosity ratio in the streamwise direction is consistent with the intermittency profile, confirming the location of the transition.

Figure 12 displays the intermittency profile along a horizontal rake located 5 mm above the surface, providing a quantitative view of the transition process. The plot shows a clear inflection near x/L = 0.3125, marking the beginning of transition, with the intermittency increasing steadily until x/L =

0.55, where it plateaus at unity, indicating fully turbulent flow. This streamwise extent accurately captures the transition region.

Finally, Figure 13 provides a direct validation of the simulation results by comparing them with experimental data from NASA Technical Report 1289 [37]. The comparison exhibits excellent agreement in velocity profile of the boundary layer in the transition location.

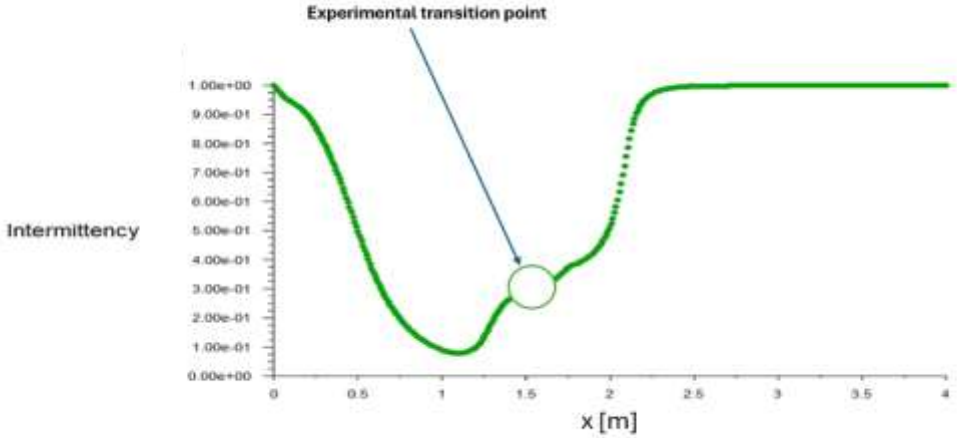

Figure 12 - Intermittency Vs x

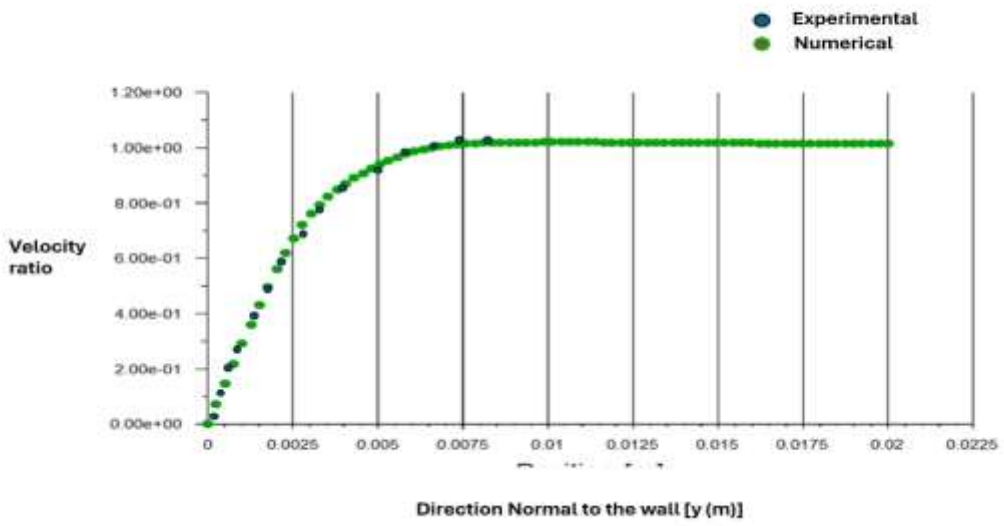

Figure 13 - Velocity Ratio Profile at transition location

Figure 13 illustrates the mean streamwise velocity profile in the transition region, extracted at a streamwise location of x/L = 0.375 from the inlet. The vertical axis represents the normalized velocity ($\frac{|\vec{U}|}{U_\infty}$), where $\vec{U}$ is the local velocity and U_∞ is the free-stream velocity, while the horizontal axis shows the wall-normal coordinate y (in meters).

This velocity profile is characteristic of transitional boundary layer flow, where the momentum transfer between the viscous sublayer and the outer inviscid flow becomes increasingly nonlinear. Starting from the wall (y = 0), the velocity gradually increases due to the no-slip condition and viscous shear, eventually reaching the free-stream value ($\frac{|\vec{U}|}{U_\infty}$ = 1) at a distance y/L ≈ 0.025. This location marks the local boundary layer thickness (δ) at x/L = 0.375, defined as the wall-normal distance at which the streamwise velocity reaches approximately 99% of the free-stream value.

4.1.2 Transition Modeling – Case 2 Flat Plate Transition at 24.38 m/s, $\boldsymbol{T_u = 0.03\%}$

In this case, the inlet velocity is increased to 24.38 m/s, while the turbulence intensity at the inlet boundary is reduced to 0.03%, representing a very low-disturbance conditions. This setup is intended to evaluate the sensitivity of the SST Transition model to variations in free-stream turbulence and to observe the corresponding delay in transition onset.

The results show a laminar boundary layer development that persists farther downstream compared to Case 1. The transition onset is observed around x/L = 0.575, followed by a gradual transition region that extends until approximately x/L = 0.725, beyond which the flow becomes fully turbulent near x/L = 0.75. This behavior aligns well with established theory, where lower turbulence intensity in the free stream tends to delay the onset of instabilities and the breakdown to turbulence.

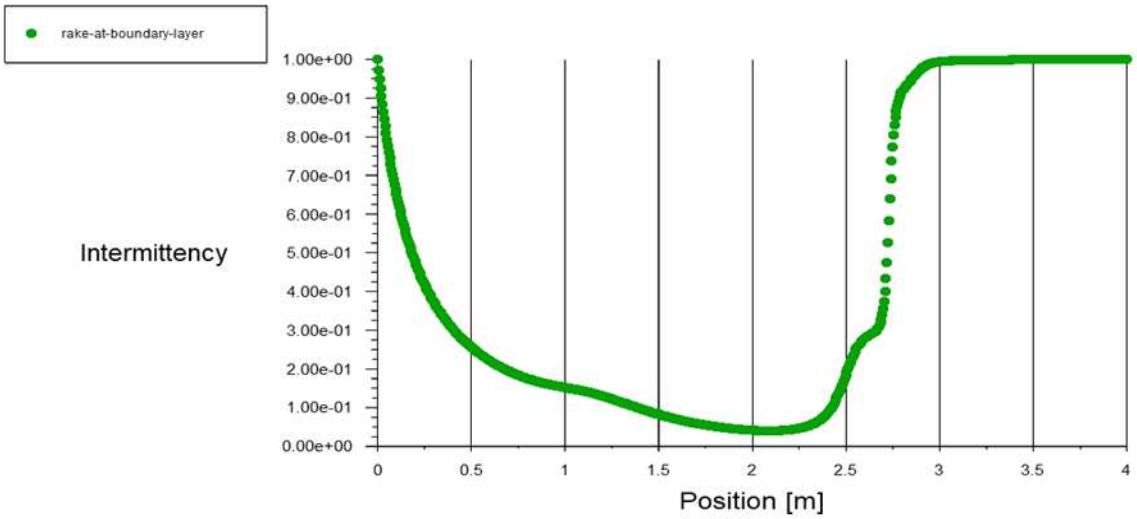

Figure 14 - Intermittency Vs x

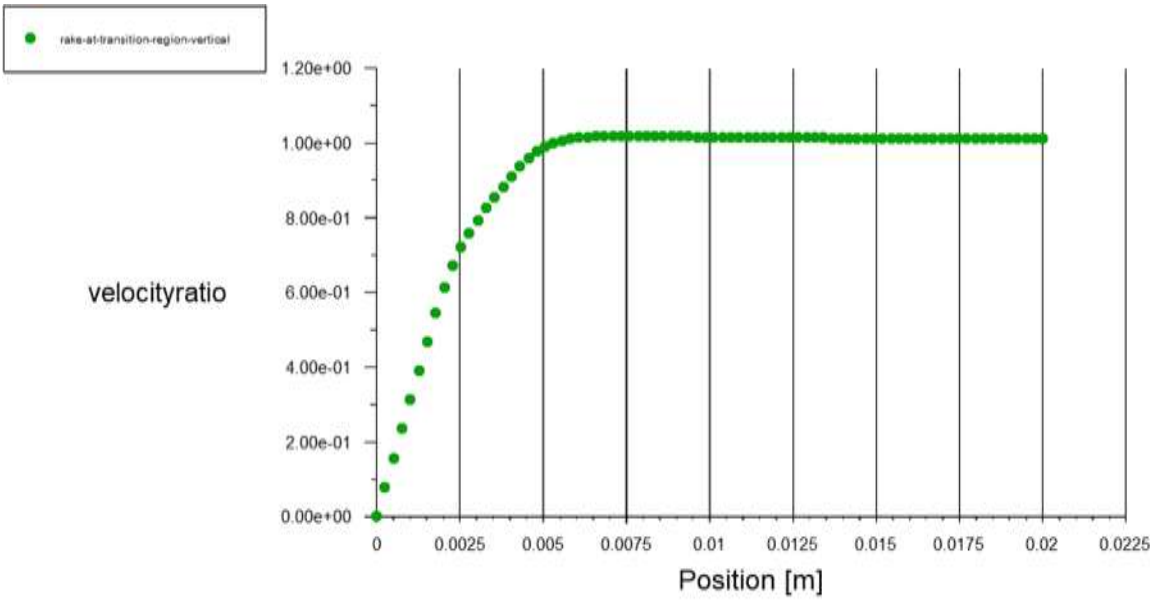

Figure 15 - Velocity Ratio Profile at transition location

Figure 15 shows the normalized velocity profile ($\frac{|\vec{U}|}{U_\infty}$) measured near the transition onset. The gradual increase in velocity from the wall to the free stream reflects the development of a transitional boundary layer. The boundary layer thickness is identified where the velocity reaches 99% of the free-stream value. These results demonstrate the SST-Transition model's capability in capturing the influence of inlet turbulence on boundary layer growth and transition prediction.

4.2 Active Flow Control Modeling

In this section, active flow control is implemented by incorporating the Shyy body force model into the momentum equations in ANSYS Fluent. This is accomplished through a UDF that injects a plasma-induced body force near the wall, mimicking the effect of a DBD plasma actuator. As described in Chapter 3, the Shyy model provides a computationally efficient method to represent the EHD force generated by the actuator without requiring the full resolution of plasma physics.

Several key parameters must be defined within the Shyy model to accurately replicate the physical behavior of the actuator. These include the maximum electric field strength (E_0), the actuation region's position (x), frequency (f), and the net charge density (q_c). The appropriate choice of these parameters is essential for ensuring the simulated flow behavior matches experimental observations, particularly in the near-wall region where plasma-body interactions are most influential.

As a baseline, we begin by applying active flow control to the first verification case, which corresponds to the NASA Technical Report 1289 [37], with a freestream velocity of 10.66 m/s and a turbulence intensity of 1%. The initial values of the Shyy model parameters used in this setup are summarized in Table 2. In subsequent sections, we will systematically vary critical parameters such as the maximum electric field strength and the streamwise location of the actuator to study their influence on flow behavior, including transition delay, modification of boundary layer profiles, and reduction in skin friction.

This controlled variation enables a parametric analysis, providing insight into the sensitivity of transition control effectiveness to plasma actuation parameters. Such a framework is crucial for identifying optimal configurations for future aerodynamic applications.

Parameter	value
Net charge density	$1 * 10^{17} \frac{C}{m^3}$
Base electric field strength	$2.27 * 10^{7} \frac{V}{m}$
Electron charge	$1.6 * 10^{-19} C$
Alpha	1
AC frequency	3000 Hz
Delta-t	0.000067 s
k_1	$6.54 * 10^{9} \frac{V}{m^2}$
k_2	$13.08 * 10^{9} \frac{V}{m^2}$

Table 2 - Values of constants and parameters used in Shyy model

4.2.1 Active Flow Control for Case 1

In Case 1, as previously observed, the transition from laminar to turbulent flow initiates at approximately x = 1.5 m in the streamwise direction. For effective flow control, plasma actuators must be positioned upstream of the transition onset, yet not so far upstream that their influence diminishes due to unnecessary early activation. Placing the actuator significantly ahead of the transition zone may lead to inefficient energy usage without meaningful impact on flow stability.

The primary objective of this investigation is to identify the optimal streamwise position for a single or multiple plasma actuators in order to

effectively delay the transition. By doing so, we aim to maximize the stabilizing effect of the actuator on the boundary layer while minimizing unnecessary energy expenditure.

A secondary objective is to determine the minimum required electric field strength that achieves transition delay under the current flow conditions. This parameter is critical from a practical standpoint, particularly in applications such as aircraft and automotive systems, where energy efficiency and power limitations are important design constraints. In real-world scenarios, an actuator that can achieve transition control with lower energy input will be more viable for integration into aerodynamic surfaces.

In the following simulations, both the actuator placement and the electric field magnitude will be systematically varied to assess their influence on boundary layer behavior and transition location. The results will offer valuable insights into the trade-off between control effectiveness and energy consumption, guiding future designs of plasma-based flow control systems.

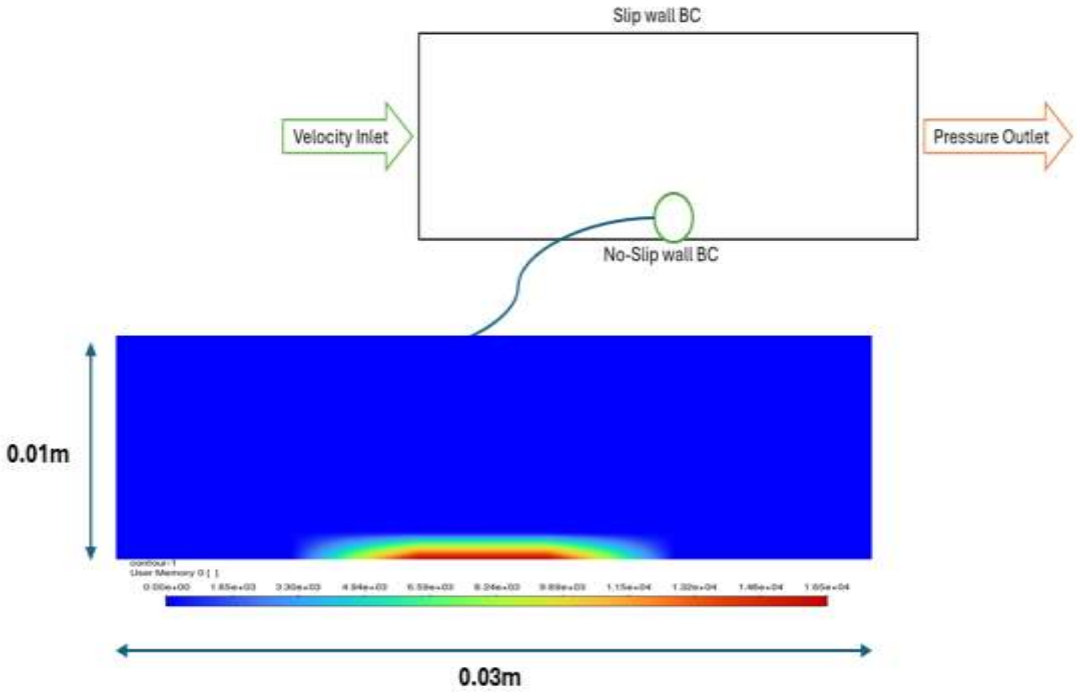

Figure 16 - Contour of electric field strength at x/L = 0.375

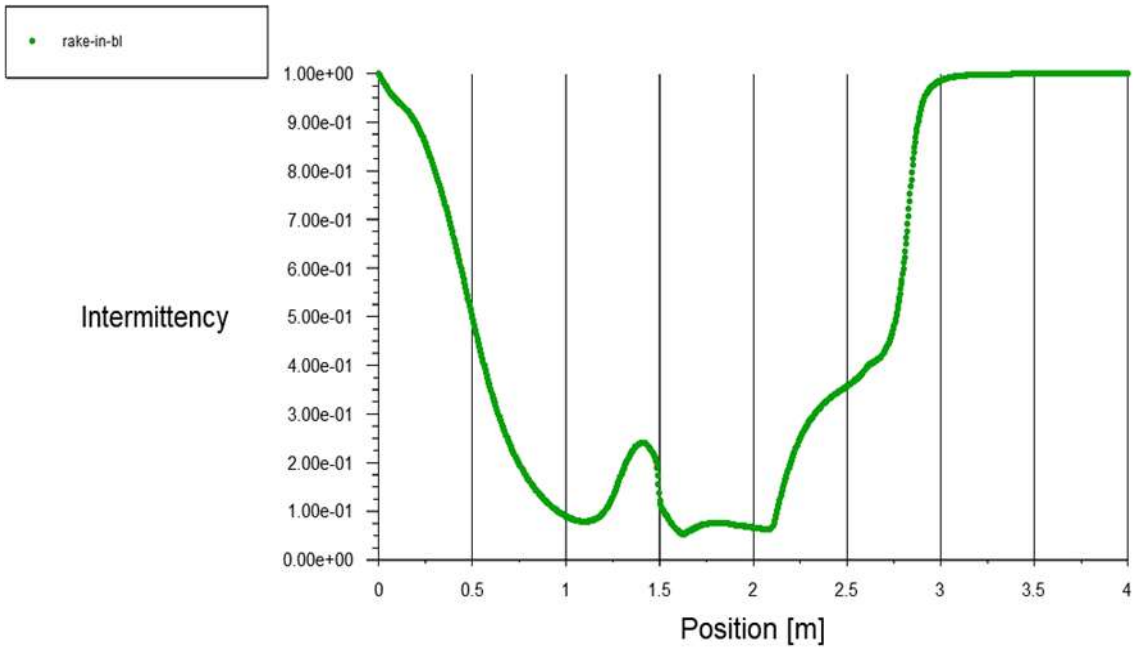

Figure 17 - Intermittency Vs x

Figure 16 illustrates the distribution and magnitude of the electric field at the actuator location, as defined by the Shyy body force model. The implementation is executed via a UDF in ANSYS Fluent, in which the electric field intensity decreases linearly with distance from the edge of the exposed electrode, in accordance with the assumptions of the model. This spatial variation in electric field strength generates a localized plasma body force that induces a jet-like flow along the surface, modifying the near-wall velocity profile.

Following the application of the body force, the impact on the boundary layer development is evident in the intermittency plot shown in Figure 17. This figure presents the intermittency distribution along a horizontal line within the boundary layer. It is observed that immediately upstream of the actuator, the intermittency value drops significantly below 0.1, indicating a re-laminarization of the flow. This laminar state persists downstream of the actuator until approximately x/L = 0.525, beyond which the intermittency gradually increases, signaling the onset of transitional flow. Compared to the baseline case without actuation, the laminar region has been extended by

more than 0.15 of x/L, demonstrating the actuator's ability to delay transition effectively.

To further assess the effect of the actuator, Figure 18 presents the intermittency contour around x/L = 0.6875, where the flow has fully transitioned to turbulence. The red coloration in the boundary layer region denotes an intermittency value approaching unity, confirming the full development of turbulent structures downstream.

The modification in the near-wall velocity profile due to plasma actuation is visualized in Figure 19, which plots the velocity ratio (local velocity divided by freestream velocity) at x/L = 0.375, coinciding with the actuator location. In the baseline scenario without flow control (refer to Figure 15), the velocity profile increases monotonically from zero at the wall to unity at the freestream, showing a classic laminar development. In contrast, the case with the actuator exhibits a sharp increase in velocity ratio near the wall, reaching approximately 0.6 almost instantaneously, followed by a slight decrease and then gradual recovery to freestream velocity. This non-monotonic behavior is indicative of the momentum injection effect from the plasma-induced body force, which accelerates the near-wall flow and alters the local shear profile. The resulting distortion in the velocity gradient affects the stability of the boundary layer, temporarily suppressing turbulence amplification.

Figure 20 displays the turbulent viscosity ratio along a streamwise line within the boundary layer. The ratio initially decreases downstream of the actuator location at x/L = 0.375, consistent with the suppression of turbulence production due to localized momentum addition. This decrease persists until around x/L = 0.55, beyond which the turbulent viscosity begins to rise, corresponding to the re-initiation of transition. After x/L = 0.625, the turbulent viscosity increases sharply, reflecting the onset of fully developed turbulence. The evolution of this parameter supports the earlier observations from intermittency and velocity plots, confirming the effectiveness of the actuator in delaying transition and modifying turbulence characteristics.

In summary, the simulation results demonstrate that a single plasma actuator, appropriately positioned near the natural transition onset, can effectively extend the laminar region, reduce turbulent kinetic energy production, and reshape boundary layer dynamics. This showcases the potential of DBD plasma actuation as a viable technique for active flow control in aerodynamic applications, particularly where transition delay and drag reduction are critical design objectives.

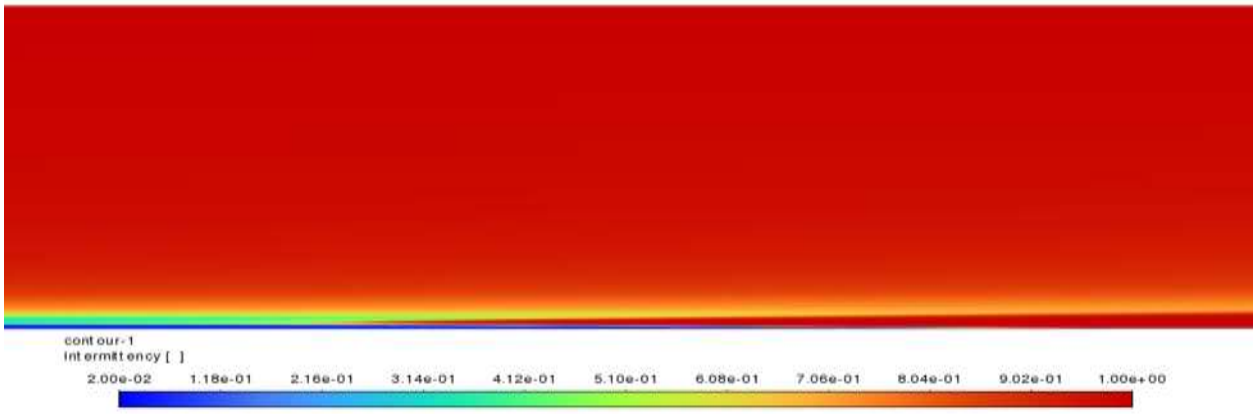

Figure 18 - Contour of Intermittency near transition location

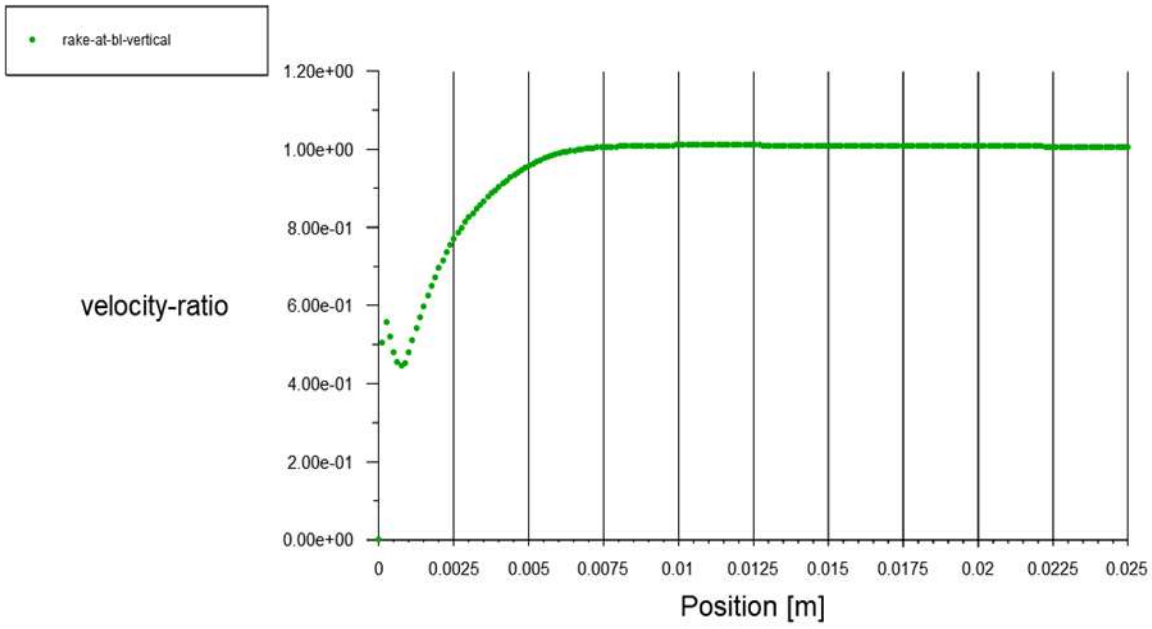

Figure 19 - Velocity Ratio Profile at Transition location

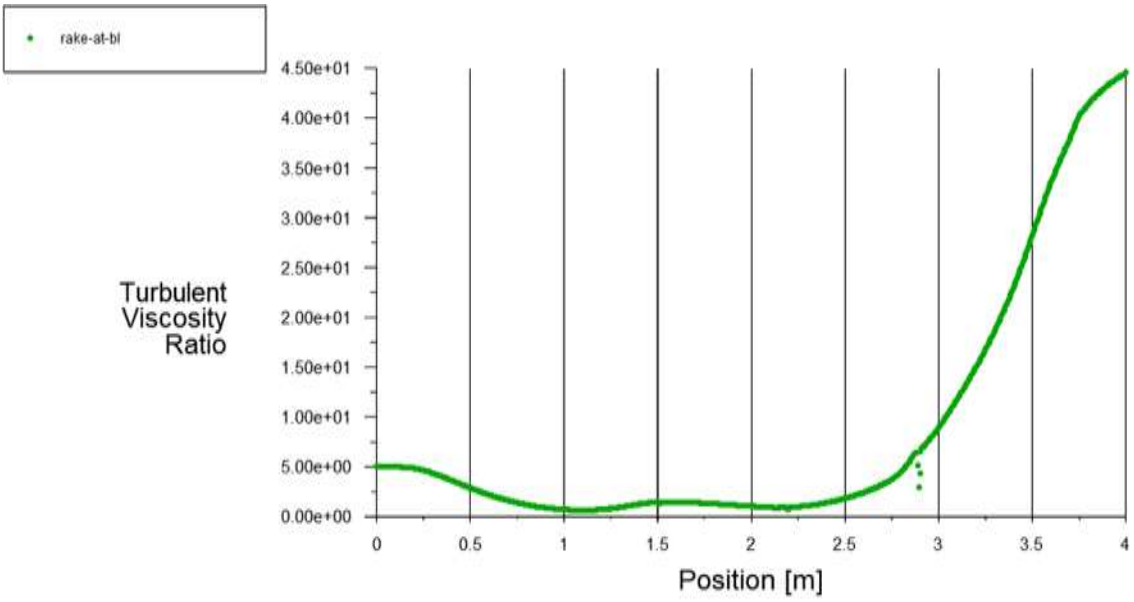

Figure 20 - Turbulent Viscosity ratio Vs x

4.2.2 Active flow control for case 2

Now we proceed to apply active flow control for Case 2, which is characterized by a freestream velocity of 24.384 m/s and a very low inlet turbulence intensity of 0.03%. In contrast to Case 1, where the turbulence intensity was significantly higher, the low turbulence levels in this case imply a more stable boundary layer, requiring a more nuanced approach to flow control. For this initial analysis, the actuator is positioned at x/L = 0.625, within the natural transition region observed in the baseline simulation for Case 2.

To establish a baseline comparison, the electric field strength is set to $2.27 * 10^7 \frac{V}{m}$, the same as used in Case 1. Figure 21 presents the intermittency distribution across the boundary layer for the entire computational domain. Contrary to the desired effect of transition delay, the intermittency increases sharply just downstream of the actuator location. This abrupt rise indicates

that the plasma actuator, instead of delaying transition, has in fact accelerated the transition process, initiating earlier turbulence development compared to the uncontrolled case.

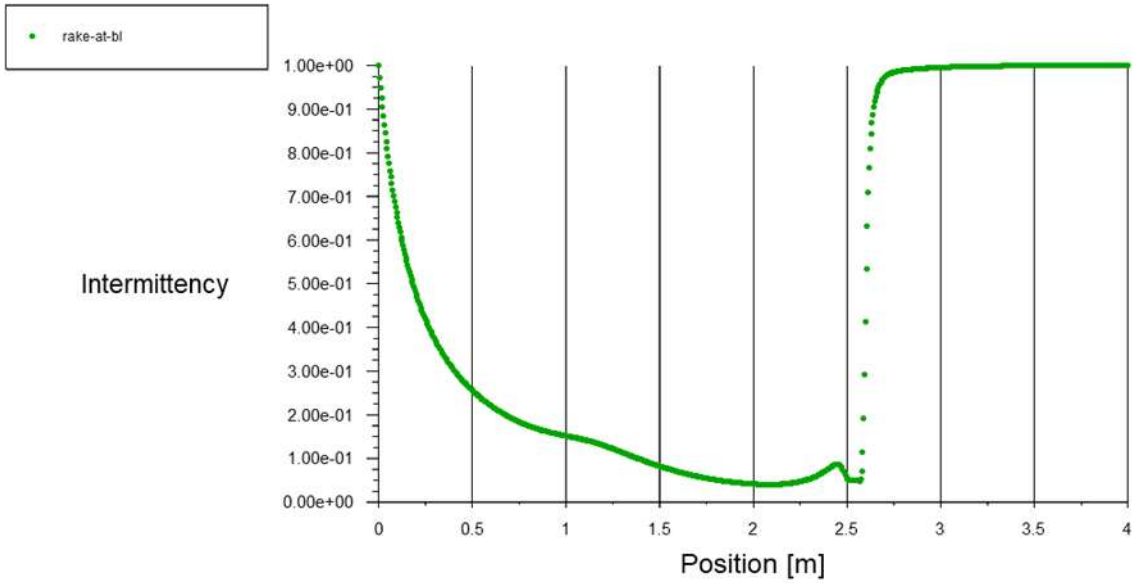

Figure 21 - Intermittency Vs x

This outcome underscores the sensitivity of low-turbulence boundary layers to external momentum addition. When the freestream turbulence intensity is low, the boundary layer is more receptive to disturbances. Introducing a high-magnitude body force into such a flow can inadvertently introduce excess kinetic energy, destabilizing the boundary layer and triggering premature transition.

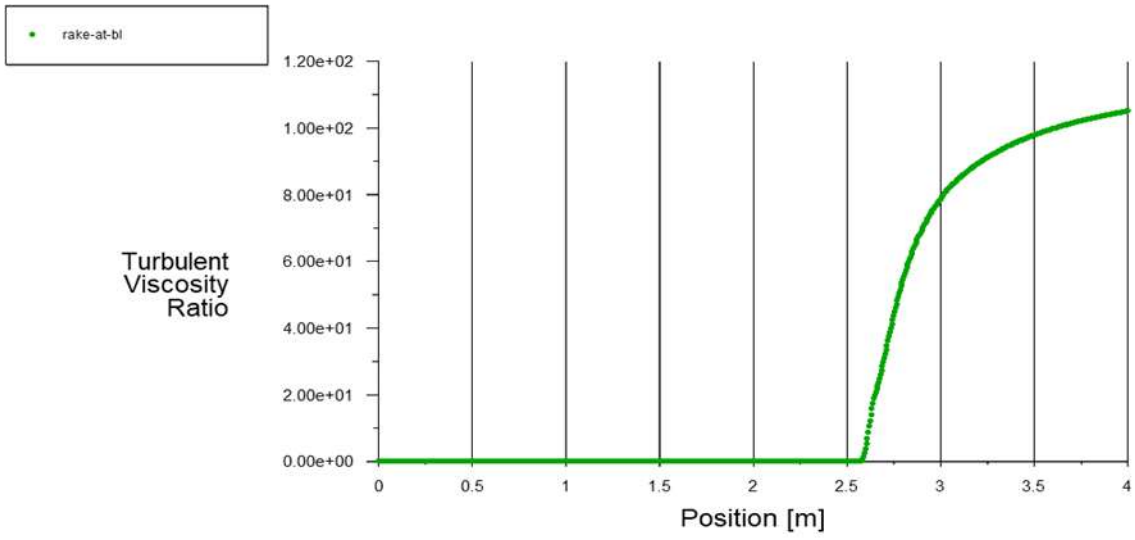

Figure 22 - Turbulent viscosity ratio Vs x

Figure 22 supports this observation by illustrating the distribution of the turbulent viscosity ratio along the boundary layer. A pronounced increase in this parameter is observed just downstream of the actuator, corresponding to the onset of turbulent structures. This behavior can be attributed to the mismatch between the actuator energy input and the baseline turbulence energy in the boundary layer. When the energy imparted by the plasma actuator exceeds the inherent turbulent energy by a large margin, it promotes early formation of coherent vortical structures, such as eddies, and leads to premature breakdown of laminar flow.

This result highlights a critical consideration in plasma flow control: actuator strength must be appropriately scaled relative to the freestream turbulence intensity and boundary layer receptivity. Unlike Case 1, where higher background turbulence could tolerate a strong actuator force without destabilization, Case 2 requires a more delicate balance. The strength of the electric field must be reduced significantly in this case to prevent undesired transition promotion.

However, there exists a physical lower limit to this reduction. The electric field cannot fall below the breakdown threshold, which is the minimum field strength required to ionize the surrounding air and initiate plasma discharge. If the applied electric field is lower than this breakdown limit, plasma generation ceases, and the actuator becomes non-functional. Therefore, the optimization process must carefully navigate between transition delay effectiveness and physical feasibility of plasma generation.

To address this, a parametric design study has been formulated to systematically vary the electric field strength while keeping all other simulation parameters constant. The goal is to identify the optimal actuation strength that achieves maximum transition delay without exceeding the stability threshold of the boundary layer. This parametric study is critical for

designing energy-efficient and effective plasma-based flow control strategies, particularly in low-turbulence flow environments such as high-altitude flights or laminar flow wings.

Parameter	E_0	$x1_{start}$	Intermittency Sum
Design Point 0	$2.27 * 10^7 \frac{V}{m}$	2.5m	508.57
Design Point 1	$1 * 10^7 \frac{V}{m}$	2.5m	531.33
Design Point 2	$7.5 * 10^6 \frac{V}{m}$	2.5m	531.33
Design Point 3	$5 * 10^6 \frac{V}{m}$	2.5m	531.33
Design Point 4	$3 * 10^6 \frac{V}{m}$	2.5m	531.33

Table 3 - Design Study for Case 2

Figure 23 presents a summary of the parametric design study conducted for Case 2. In this investigation, the only varying input parameter is the electric field strength applied by the DBD plasma actuator, while the output parameter is defined as the cumulative intermittency along a line positioned within the boundary layer, extending from the inlet to the outlet of the computational domain.

This output metric computed as the sum of the intermittency values across all computational cells along the selected line is sensitive to mesh resolution in the near-wall region. A finer mesh yields a more detailed representation of intermittency variations and a more accurate estimation of the transition extent. The cumulative intermittency essentially quantifies the overall degree of turbulence development across the domain, serving as a surrogate for measuring the effectiveness of transition delay or premature triggering under different actuation strengths.

Analysis of the results clearly indicates that the response of the boundary layer to active flow control is strongly dependent on the freestream inflow condition, particularly the turbulence intensity. In Case 2, where the

turbulence intensity is extremely low (0.03%), applying plasma actuation with a high electric field strength introduces a substantial and abrupt addition of momentum to an otherwise stable boundary layer. This artificial momentum injection promotes the formation and growth of vortical structures, which accelerates the transition to turbulence rather than suppressing it.

This behavior is consistent with bypass transition mechanisms, where disturbances such as streaks or vortices generated by the actuator can rapidly grow and destabilize the laminar boundary layer. Since the natural flow in Case 2 exhibits minimal initial turbulence, the plasma body force acts as a dominant disturbance source, directly triggering premature transition.

In contrast, Case 1 with a higher turbulence intensity of 1% presents a fundamentally different flow regime. Here, the boundary layer already contains pre-existing turbulent structures, and the application of the same actuator strength serves to reorganize and suppress these instabilities, thereby delaying the transition process. In this case, the actuator reinforces flow stability, and only one actuator is sufficient to extend the laminar region by more than 0.15 x/L.

These findings highlight an important design principle: the effectiveness of plasma-based active flow control is not universal, but highly sensitive to the inflow turbulence level. While high-strength actuation can suppress transition in disturbed flows, the same input may destabilize low-turbulence boundary layers and act counterproductively. Therefore, tailoring actuator strength to the background flow conditions is crucial to achieving effective and energy-efficient flow control.

This case study also underscores the need for adaptive control strategies, where plasma actuation parameters such as voltage, frequency, or actuation timing are dynamically tuned based on real-time flow diagnostics. Such strategies are essential for deploying plasma actuators in practical applications, including aircraft wings, wind turbines, and low-drag vehicle design, where flow conditions are constantly changing.

4.3 Optimization Setup of Case 1

As discussed in the previous sections, Case 1 demonstrated a substantial delay in boundary layer transition when active flow control using a DBD plasma actuator was applied. Based on the Shyy body force model, two parameters play a dominant role in this transition delay: the maximum electric field strength (which correlates with actuator voltage) and the streamwise location of the actuator. To identify the optimal combination of these two critical parameters, an optimization study was conducted within the ANSYS Workbench environment.

The optimization process utilized the Response Surface Methodology (RSM), a robust statistical and mathematical technique designed to approximate complex relationships between input parameters and system responses. RSM serves as a surrogate modeling approach, enabling engineers and researchers to explore the design space without conducting an exhaustive number of expensive CFD simulations.

In this context, the response surface is generated using a selected number of full CFD simulations, each corresponding to a unique pair of actuator location and electric field strength. The results of these simulations are then used to fit an approximate model (typically a second-order polynomial, Kriging, or radial basis function) that captures the underlying behavior of the system. Once constructed, this surrogate model can be used for sensitivity analysis, design exploration, and optimization, significantly reducing computational overhead.

A crucial aspect of this methodology is the Design of Experiments strategy, which determines how sample points are selected in the input parameter space. To ensure the accuracy and generalizability of the response surface, an Optimal Space-Filling Design (OSFD) was adopted. This approach guarantees that the sample points are uniformly distributed across the design space, capturing both local and global variations in system behavior.

In this study, the OSFD employed advanced sampling techniques such as Latin Hypercube Sampling (LHS) or Sobol sequences, which are known for their ability to minimize point clustering and maximize coverage of the design domain. These techniques ensure that even with a limited number of

simulations, the surrogate model remains representative and predictive. The advantage of this method is twofold: first, it minimizes computational cost by reducing the number of full-scale CFD simulations required. Second, it allows for robust multi-objective optimization, making it possible to balance performance improvement (e.g., maximum transition delay) with practical constraints such as energy consumption (related to electric field strength).

As shown in Table 3, a Design of Experiments was conducted using two key input parameters: the maximum electric field strength of the plasma actuator and its streamwise starting location along the flat plate. These two variables were selected based on their direct influence on the effectiveness of transition delay, as previously demonstrated in Case 1.

Two output (response) parameters were defined to evaluate the performance of each design configuration. The first output is the summation of intermittency values along a monitoring line located at y/L = 0.016 in the normal direction from the bottom wall. This line extends from the inlet to the outlet along the streamwise direction. The summation of intermittency values across this line provides a quantitative measure of the transition region's development, as lower intermittency values generally correspond to more laminar flow. It is important to note that this metric is mesh-dependent, as the value is calculated by integrating intermittency across discrete cells intersected by the probe line.

Parameter	E_0	$x1_{start}$	Intermittency summation	Skin friction integral
Design Point 1	$3.88 * 10^7 \frac{V}{m}$	1.16m	226.74	0.0068
Design Point 2	$4.77 * 10^7 \frac{V}{m}$	1.38m	183.09	0.0071
Design Point 3	$2.11 * 10^7 \frac{V}{m}$	1.72m	739.22	0.0081
Design Point 4	$3.44 * 10^7 \frac{V}{m}$	1.61m	346.47	0.0074
Design Point 5	$1.66 * 10^7 \frac{V}{m}$	1.05m	741.71	0.0081

Design Point 6	$2.55 * 10^7 \frac{V}{m}$	1.27m	321.54	0.0057
Design Point 7	$3 * 10^7 \frac{V}{m}$	1.94m	321.14	0.0064
Design Point 8	$4.33 * 10^7 \frac{V}{m}$	1.83m	695.56	0.0105
Design Point 9	$1.22 * 10^7 \frac{V}{m}$	1.5m	741.21	0.0081

Table 4 - Design study for optimization of case 1

The second output parameter is the integral of the skin friction coefficient (Cf) over the bottom surface of the domain, which is defined as a no-slip wall boundary. This integral provides a global measure of wall shear stress, which is strongly influenced by boundary layer state, higher skin friction typically indicates more turbulent flow, while lower values suggest laminar or transitional behavior. Together, these two outputs offer complementary insights into both the internal flow development and surface interaction effects of the actuator, making them suitable objective functions for the subsequent response surface construction and optimization.

As illustrated in Table 4, a Design of Experiments was performed using two input parameters: the maximum electric field strength (E_0) of the plasma actuator and its starting location along the flat plate ($\boldsymbol{x1_{start}}$). These parameters were chosen due to their direct influence on the actuator's effectiveness in delaying the laminar-to-turbulent transition.

The ultimate objective of this study is to maximize transition delay, thereby preserving laminar flow for as long as possible. This strategy reduces viscous drag over most of the surface. However, it is important to note that the actuator itself introduces a strong localized momentum injection into the boundary layer. As a result, skin friction rises sharply in the actuator region, potentially offsetting some of the global drag-reduction benefits.

From the DOE results, it is evident that the global minima of the two output functions occur at different design points. For instance, the lowest intermittency summation occurs at Design Point 2, where the electric field strength is approximately $4.77 * 10^7\ V/m$. This value is notably higher than

that used in the original Case 1 simulation. In contrast, the minimum skin friction integral is observed at Design Point 6, corresponding to an electric field of $2.55 * 10^7\ V/m$. This discrepancy highlights an important consideration in multi-objective optimization: depending on which metric is prioritized (transition delay or drag reduction), the optimal design configuration will vary.

Since the primary goal of this investigation is to delay the transition rather than minimize skin friction directly, the intermittency summation has been selected as the objective function for the subsequent optimization. The Multi-Objective Genetic Algorithm within ANSYS Workbench is used to optimize the response surface based on this criterion. This approach allows for an effective search of the design space while accounting for nonlinear interactions between input parameters and transition behavior.

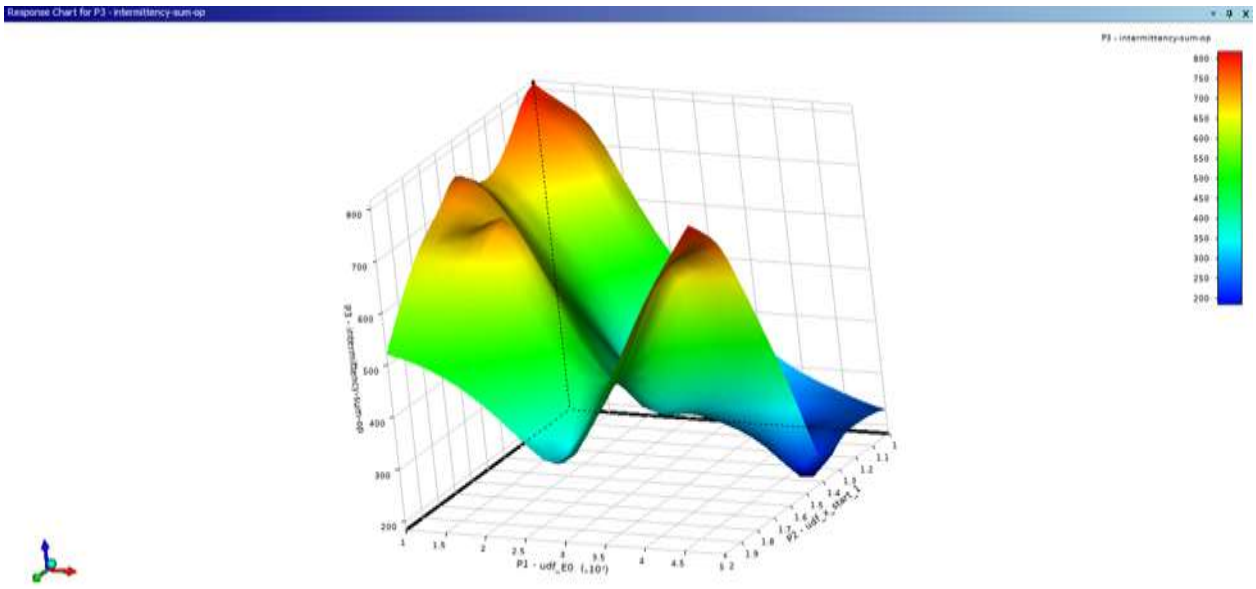

Figure 23 - Response Surface

The trade-off chart presented in Figure 24 illustrates the relationship between two key performance indicators in the context of plasma-based active flow control: the intermittency summation within the boundary layer and the integral of the skin friction coefficient along the wall. This plot offers

a visual representation of the inherent trade-off between delaying transition and minimizing drag.

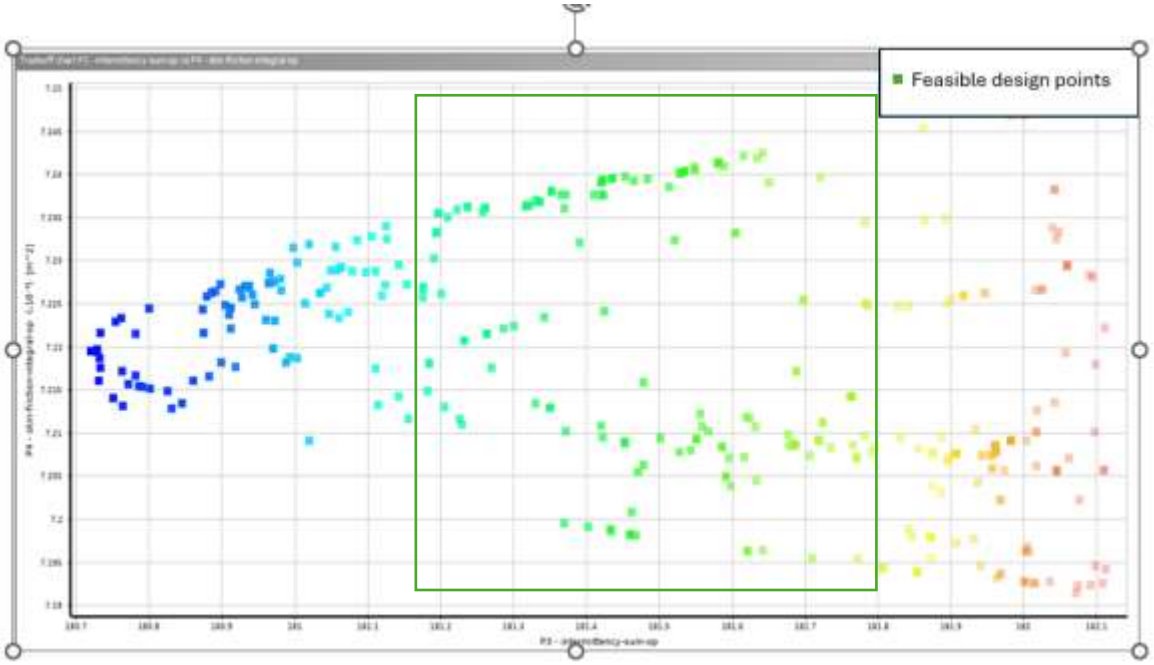

Figure 24 - Tradeoff Between two different output parameters

The horizontal axis represents the total intermittency value. Lower values indicate a more laminar boundary layer, while the vertical axis displays the integrated skin friction coefficient, which reflects the total viscous drag on the surface. Green points show feasible design points where both of these output functions are satisfied. Since the points are scattered in the plot, it implies that there is no linear relationship between these output functions.

As expected, designs with higher intermittency summation indicative of earlier transition tend to exhibit higher skin friction integrals, confirming that premature turbulence leads to increased viscous losses. Conversely, lower intermittency values correspond to extended laminar flow and reduced wall shear stress, except in localized regions near the actuator where momentum injection temporarily increases shear forces.

From this trade-off analysis, a candidate design point was identified that achieves the lowest intermittency summation.

Optimal actuator position	Optimal electric field strength
1.36m	$4.74 * 10^7 \frac{V}{m}$

Table 5 - Optimal Design Point

This configuration positions the plasma actuator upstream of the natural transition onset, enabling the generated body force to interact with the developing boundary layer before turbulent spots fully form. The placement is critical: it ensures that momentum is introduced into the flow early enough to dampen instabilities and reduce disturbance amplification, effectively delaying the transition to turbulence. The result demonstrates that intelligent placement and tuning of actuator parameters, particularly electric field strength and location can achieve substantial gains in laminar flow preservation, with penalties in drag increase due to local plasma-induced shear. This optimized design forms the basis for further investigations into multi-actuator systems, unsteady flow regimes, or geometry-sensitive control strategies, where trade-offs may be even more complex and critical to system-level performance.

4.4 Optimization Setup of Case 1 with Two Actuators

Following the successful optimization of a single DBD plasma actuator configuration, the present study extends the investigation by incorporating a dual-actuator system. The primary objective of this phase is to assess whether the introduction of a second actuator can further improve control over the laminar-to-turbulent transition on a flat plate. The hypothesis is that a multi-actuator strategy may offer enhanced boundary layer stabilization by more effectively redistributing momentum, delaying the onset of turbulence, and modifying disturbance growth in a more controlled and localized manner.

The inclusion of a second actuator introduces additional degrees of freedom into the optimization framework, such as: The relative spacing between actuators, Their individual streamwise placement along the surface, and the potential for tuning electric field strengths independently. However, to limit

computational complexity in the initial study, both actuators were assigned the same electric field strength, mirroring the value used in the single-actuator optimized case. This assumption simplifies the parameter space while still allowing meaningful insights into the benefits of multiple actuators. Also having one high voltage source seems more feasible when dealing with this problem experimentally.

For the baseline dual-actuator configuration, three input parameters were defined: $\boldsymbol{x1_{start}}$ the streamwise position of the first actuator, $\boldsymbol{x2_{start}}$ the streamwise position of the second actuator and the maximum electric field strength (assumed identical for both actuators).

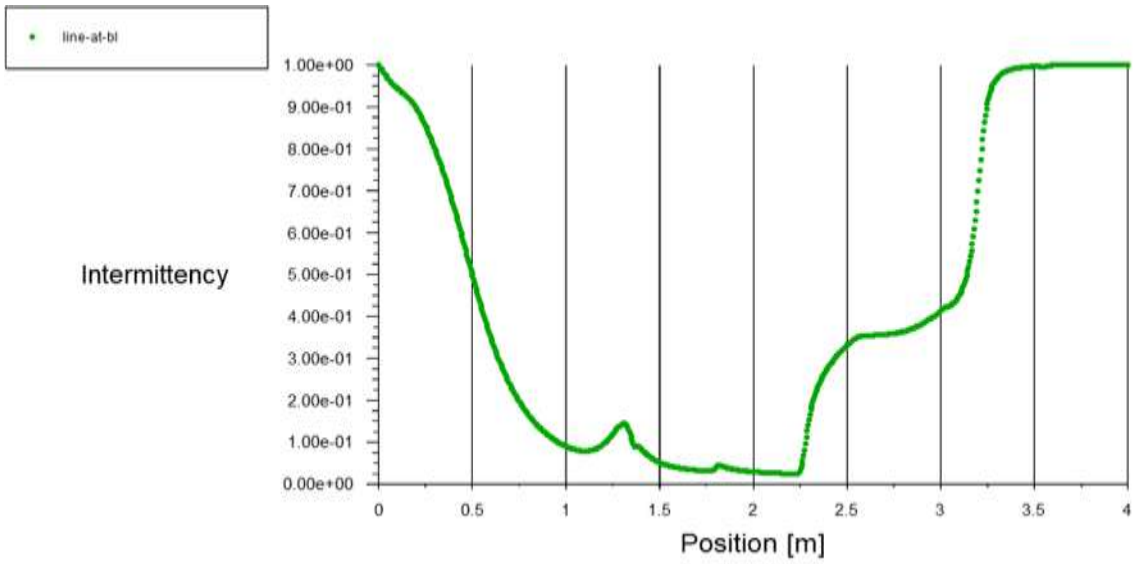

Figure 25 - Intermittency Vs x

The intermittency distribution resulting from the dual-actuator simulation is presented in Figure 25. As observed, the application of two plasma actuators leads to a significant suppression of intermittency across an extended portion of the boundary layer when compared to the uncontrolled baseline case. The first actuator, positioned upstream, introduces an early injection of momentum, which attenuates small disturbances and delays the initial stages of transition. The second actuator, located further downstream, serves to reinforce the stabilization effect, suppressing residual instabilities and further postponing the laminar-to-turbulent

transition. This cumulative effect produces a broader laminar region, highlighting the effectiveness of a distributed flow control strategy.

This base case with two actuators establishes a reference configuration for the optimization phase. In that phase, the positions of the actuators and the electric field strength will be fine-tuned to achieve minimum intermittency integral throughout the domain. The main objective is to maximize the extent of laminar flow, which directly contributes to drag reduction, while maintaining the electric field strength within physically realizable limits to ensure energy efficiency and actuator feasibility in real-world implementations.

The distribution of the skin friction coefficient (Cf), shown in Figure 26, provides further insight into the impact of the dual-actuator configuration on boundary layer behavior. The profile initially displays a sharp decline, typical of laminar boundary layers, as the flow accelerates from the stagnation point. Notably, two distinct local peaks in Cf are observed, coinciding precisely with the positions of the plasma actuators. These peaks represent localized increases in wall shear stress; a direct result of the momentum injection associated with the body force generated by each actuator.

These localized energizations temporarily strengthen the near-wall velocity gradient, helping to stabilize the flow and delay separation and transition. Beyond the second actuator, the skin friction coefficient gradually increases, indicating that the flow begins to recover and transition, though at a downstream location relative to the single-actuator case. This spatial delay is a clear indication of the effectiveness of distributed plasma forcing in maintaining laminar conditions over a larger surface area.

Together, the intermittency and skin friction data confirm the potential of multi-actuator strategies in enhancing active flow control performance, setting the stage for further optimization and design studies.

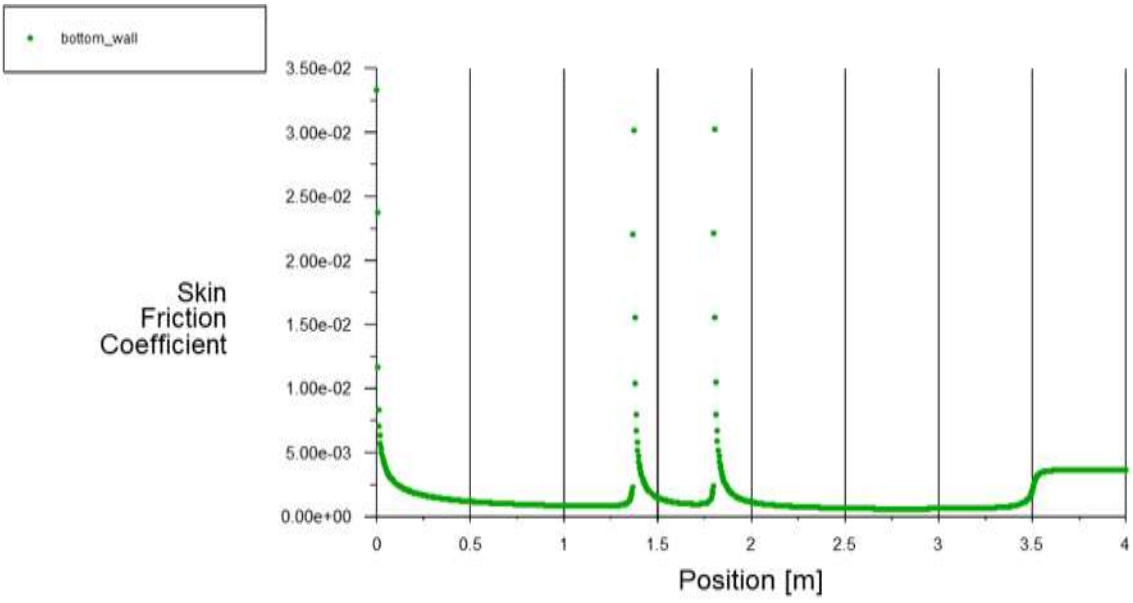

Figure 26 - Skin friction coefficient Vs x

The Design of Experiments Table, shown in Figure 29, summarizes the results of 15 simulation cases conducted to investigate the influence of three critical input parameters on flow control effectiveness using a dual DBD plasma actuator configuration. The chosen DoE framework allows for systematic variation and analysis of the input design space, enabling the identification of optimal combinations for transition delay.

The input parameters varied across the following ranges:

- ✓ Electric field strength of the plasma actuators: from $1 * 10^7 \frac{V}{m}$ to $5 * 10^7 \frac{V}{m}$
- ✓ Starting location of Actuator 1: from 0.25 x/L to 0.625 x/L
- ✓ Starting location of Actuator 2: from 0.25 x/L to 0.625 x/L

These ranges were selected based on preliminary single-actuator optimization results and practical constraints related to actuator placement and energy limits. The decision to keep the same electric field strength for both actuators was made to reduce the computational complexity of the design space while still capturing the essential trends in flow behavior.

Parameter	$E_0[\frac{V}{m}]$	$x1_{start}$[m]	$x2_{start}$[m]	Intermittency summation
Design Point 1	$4.33 * 10^7$	1.25	2.15	577.56
Design Point 2	$2.46 * 10^7$	1.15	2.25	263.7
Design Point 3	$1.4 * 10^7$	1.95	2.15	547.37
Design Point 4	$4.06 * 10^7$	1.15	2.05	199.37
Design Point 5	$1.13 * 10^7$	1.25	1.85	547.68
Design Point 6	$4.86 * 10^7$	1.55	1.55	605.08
Design Point 7	$3.53 * 10^7$	1.05	1.45	207.49
Design Point 8	$4.6 * 10^7$	1.85	2.25	537.34
Design Point 9	$3.26 * 10^7$	1.65	1.65	288.76
Design Point 10	$3 * 10^7$	2.05	2.45	475.34
Design Point 11	$1.93 * 10^7$	1.75	2.45	531.91
Design Point 12	$1.66 * 10^7$	1.35	1.75	505.49
Design Point 13	$2.73 * 10^7$	1.05	1.45	288.77
Design Point 14	$3.8 * 10^7$	1.95	2.35	454.9
Design Point 15	$2.2 * 10^7$	1.35	2.35	383.2

Figure 27 - Design study for the case with two actuators

The output parameter used for evaluating flow control performance is the summation of the intermittency values along a horizontal line located inside the boundary layer. This line extends from the inlet to the outlet at a fixed height of 0.016 y/L above the wall, intersecting all near-wall cells. The

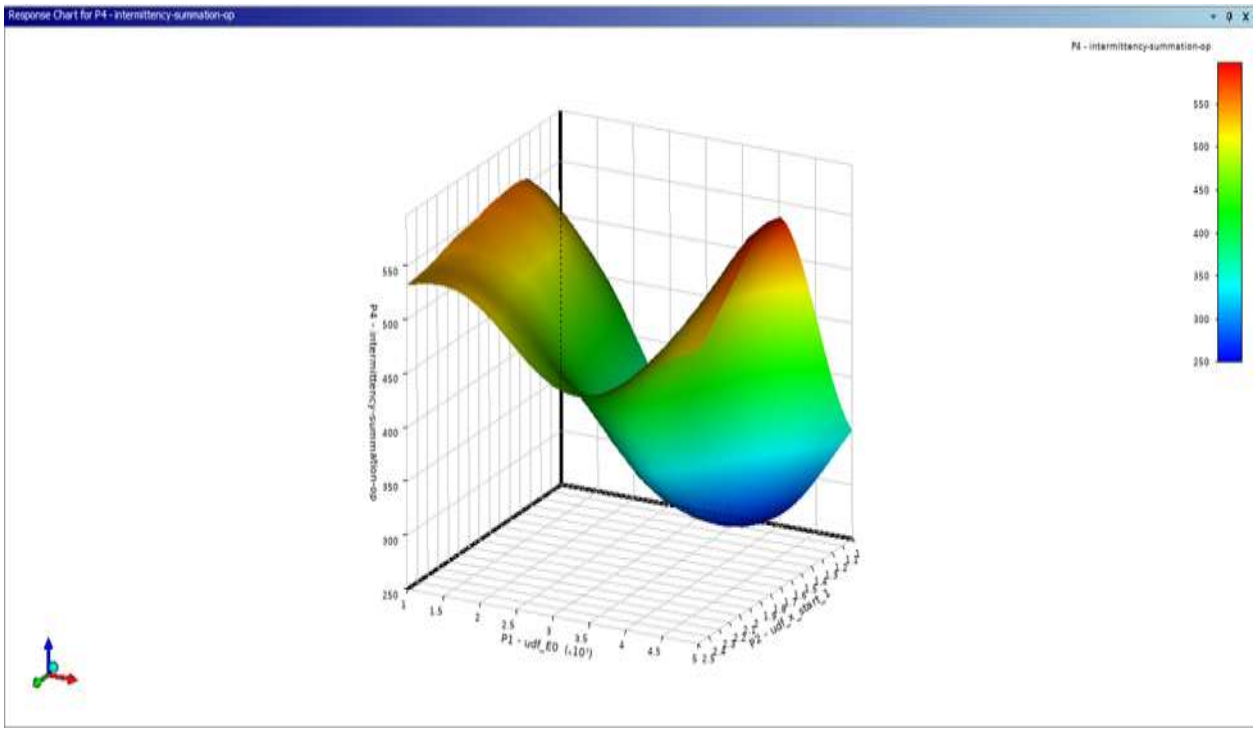

Figure 28 - Response Surface of Design study

Figure 28 presents the response surface generated from the input and output parameters for the dual plasma actuator configuration. This surface provides a valuable visualization of the nonlinear relationship between the electric field strength and the starting locations of both actuators with respect to their influence on transition delay, as quantified by the intermittency summation metric.

The analysis of the response surface reveals that effective transition control cannot be achieved by tuning the electric field or actuator position in isolation; instead, an optimized combination of both parameters is required. Specifically, the surface indicates that moderate electric field strengths, when coupled with strategically chosen actuator positions, lead to maximum delay of the laminar-to-turbulent transition. At lower electric field strengths, shifting the actuator positions results in only marginal improvements. However, at medium to high field strengths, the placement becomes far more sensitive, underscoring the importance of precise actuator positioning for effective momentum injection and suppression of transition-triggering disturbances. From the design space, the following optimal configuration was identified:

Optimal position of first actuator	Optimal position of second actuator	Optimal electric field strength
1.06m	2.04m	$3.93 * 10^7 \frac{V}{m}$

This combination corresponds to one of the lowest intermittency summation values across all tested design points, implying a significant extension of the laminar flow region along the flat plate. The first actuator, placed upstream near the natural transition onset, plays a critical role in suppressing initial instability waves, thereby shifting the onset of transition downstream. The second actuator, positioned further along the plate, acts to stabilize the developing boundary layer and reinforce laminar behavior, preventing re-transition due to pressure recovery region where flow decelerates after first actuator.

The chosen electric field strength falls within the moderate to high range. While higher values of electric field strength may seem attractive, they were observed to yield diminishing returns in terms of transition control, and in some cases even promote early turbulence due to excessive momentum addition. Conversely, lower field strengths were insufficient to trigger a meaningful flow response. Thus, the selected value is both aerodynamically effective and practically feasible, respecting the operational limits of plasma actuators in real-world flow control systems.

In summary, the response surface analysis confirms that dual-actuator systems, when appropriately optimized, offer superior flow control performance over single-actuator configurations. The identified optimal setup ensures extended laminar flow, reduced skin friction, and improved aerodynamic efficiency, key objectives in modern fluid dynamics and control-oriented aerodynamic design.

Chapter 5: Conclusion

This thesis investigated the implementation and optimization of DBD plasma actuators as an active flow control method to delay laminar-to-turbulent transition over a flat plate. A comprehensive numerical framework was developed, incorporating advanced turbulence modeling, custom body force modeling via a UDF, and parametric and multi-objective optimization using ANSYS Fluent and Workbench.

The study began by validating the transition SST 4-equation model in ANSYS Fluent through a series of test cases, which varied inlet velocity and turbulence intensity to replicate transition phenomena under different freestream conditions. The simulations showed strong agreement with experimental data from NASA Report 1289 [37], particularly in terms of transition region and velocity profiles across the boundary layer. This verification step established confidence in the numerical approach before applying any active control strategies.

Shyy body force model was then implemented in the Navier–Stokes equations through a UDF to simulate the localized body force generated by plasma discharge. The Shyy model was selected due to its computational efficiency, ease of integration into commercial CFD solvers, and reasonable agreement with experimental trends in literature. Its simplified representation of plasma-induced body force, assuming a linear electric field distribution and empirically defined charge density enabled the simulation of plasma effects without solving the full set of Maxwell's equations or plasma transport equations, thereby reducing computational cost substantially.

Findings from Active Flow Control Implementation

Two baseline cases were selected to evaluate the effect of plasma actuators on transition dynamics:

- ✓ **Case 1:** Inlet velocity of 10.668 m/s and turbulence intensity of 1%
- ✓ **Case 2:** Inlet velocity of 24.384 m/s and turbulence intensity of 0.03%

For Case 1, the implementation of a single plasma actuator led to a transition delay of more than 0.15 x/L, a significant improvement in maintaining laminar flow. The intermittency plots, turbulent viscosity ratio contours, and velocity profiles confirmed the extension of the laminar boundary layer region. The actuator effectively energized the near-wall fluid, reducing susceptibility to perturbation growth and delaying transition.

Conversely, in Case 2, using the same electric field strength as Case 1 led to premature transition. Due to the lower turbulence intensity, the boundary layer was more susceptible to being destabilized by the actuator's momentum addition. This key finding highlighted that plasma actuation must be carefully tuned to the background turbulence level. High energy input under very low turbulent conditions can inadvertently trigger transition by introducing unsteady structures that amplify downstream.

Optimization of Actuator Parameters

A detailed parametric study and optimization process was conducted for Case 1 to identify the optimal configuration for the actuator. The response surface methodology was employed using ANSYS Workbench's Design of Experiments and Multi-Objective Genetic Algorithm. The optimization problem aimed to minimize the intermittency summation across the boundary layer.

The optimization process revealed the following optimal single-actuator configuration:

Optimal actuator position	Optimal electric field strength
1.36m	$4.74 * 10^7 \frac{V}{m}$

This configuration achieved the best performance in early instability suppression, leading to substantial transition delay. Trade-off analysis confirmed that while drag slightly increased locally due to the actuator, the overall laminar flow region was significantly extended.

To further enhance performance, the study was extended to investigate a dual actuator configuration. The objective was to explore whether combining two actuators, each contributing localized momentum injection, could achieve a more robust and extended laminar regime. The base case with two actuators placed at x/L = 0.3425 and x/L = 0.45 showed improved control of the boundary layer. Two distinct peaks in the skin friction coefficient curve confirmed effective momentum addition. Intermittency distribution indicated extended laminar flow region, particularly in the region between and downstream of the actuators. Following a second round of response surface optimization, the following optimal dual-actuator configuration was identified:

Optimal position of first actuator	**Optimal position of second actuator**	**Optimal electric field strength**
1.06m	2.04m	$3.93 * 10^7 \frac{V}{m}$

This configuration yielded one of the lowest intermittency summations recorded in the entire study, confirming the effectiveness of dual-actuator arrangements in extending laminar flow. The dual setup allowed for early suppression of disturbances and reinforcement of laminarity further downstream, compensating for pressure recovery region and flow instabilities that may arise after the first actuator's influence diminishes.

Scientific and Engineering Contributions

This thesis makes several key contributions to the field of plasma-based flow control:

1. Implementation of a simplified plasma body force model (Shyy) into a commercial CFD solver, enabling fast parametric studies without expensive plasma solvers.
2. Demonstration of plasma actuator impact under different turbulence intensities, revealing that inappropriate parameter choices can trigger early transition, especially under low-disturbance conditions.
3. Development of a robust optimization workflow using response surface methods and genetic algorithms to fine-tune actuator placement and intensity.
4. Validation of dual-actuator strategies, which show improved transition control compared to single-actuator setups, highlighting the potential for multi-point plasma control in real aerodynamic applications.

Limitations and Recommendations for Future Work

While the study provided insightful results, several limitations must be acknowledged:

- The Shyy model, although efficient, assumes a linear electric field distribution and constant charge density, which may not fully capture complex plasma-fluid interactions.
- The simulations were performed in 2D, which may neglect important spanwise dynamics and three-dimensional instability mechanisms which are negligible in the case of a flat plate but become important when dealing with swept wing or asymmetric flow configurations.
- The energy consumption analysis was qualitative. A more detailed electrical model could improve estimation of actuator power input and efficiency.

For future research, the following directions are recommended:

- Coupling with electrostatic solvers or simplified plasma transport equations for more accurate body force estimation.
- Inclusion of realistic voltage waveforms, including pulsed and modulated signals, to investigate their role in actuator efficiency.
- Investigating the effects of AC signal frequency on actuator performance.
- Investigating energy consumption of various configurations.
- Experimental validation in wind tunnel setups to complement and verify simulation-based results.

In conclusion, this thesis has demonstrated that DBD plasma actuators, when properly configured and optimized, can significantly delay boundary layer transition on a flat plate, contributing to extended laminar flow region. The findings provide a strong foundation for future implementation of plasma-based flow control strategies in aerospace and automotive systems.

Appendix A: UDF Code

```
#include "udf.h"

#define NUM_ELECTRODES 1  // Number of electrodes

// Global variables
real E0;                          // Base electric field parameter (from Fluent
input)
real k1;                          // Constant for electric field calculation
(set to 6.54e9)
real k2;                          // Constant for electric field calculation
(set to 13.08e9)
real REGION_X_START[NUM_ELECTRODES]; // Starting x-coordinate for each
electrode region
real REGION_X_END[NUM_ELECTRODES];   // Ending x-coordinate for each electrode
region (calculated as x_start + 0.01)
int ELECTRODE_STATUS[NUM_ELECTRODES]; // Electrode status: always 1 (active)

// Other defined constants
#define CHARGE_DENSITY 1.0e17       // Charge density (SI units)
#define ELECTRON_CHARGE 1.6e-19     // Electron charge (SI units)
#define ALPHA 1.0                   // Coefficient multiplier
#define frq 3000.0                  // Frequency (Hz)
#define delta_t 0.000067            // Time step (s)
#define REGION_Y_START 0.0          // Lower y-bound for electrode region
#define REGION_Y_TOP 0.003          // Upper y-bound for electrode region

/*---------------------------------------------------------------
  Function: calculate_electric_field_x
  Purpose:  Calculates the x-component of the electric field at a given
            (x,y) location for a specified electrode.
---------------------------------------------------------------*/
real calculate_electric_field_x(real x, real y, int electrode_index)
{
    return (E0 - k1 * (x - REGION_X_START[electrode_index]) - k2 * y) *
        (k2 / sqrt(k1 * k1 + k2 * k2));
}

/*---------------------------------------------------------------
  Function: calculate_electric_field_y
  Purpose:  Calculates the y-component of the electric field at a given
            (x,y) location for a specified electrode.
---------------------------------------------------------------*/
real calculate_electric_field_y(real x, real y, int electrode_index)
{
    return (E0 - k1 * (x - REGION_X_START[electrode_index]) - k2 * y) *
        (k1 / sqrt(k1 * k1 + k2 * k2));
}

/*---------------------------------------------------------------
  UDF: body_force_x
  Purpose:  Computes the x-direction source term due to electric field.
            All electrodes are active (status = 1).
---------------------------------------------------------------*/
DEFINE_SOURCE(body_force_x, cell, thread, dS, eqn)
{
    real x[ND_ND];              // Cell centroid coordinates
    real electric_field_x[NUM_ELECTRODES];
    real source_term = 0.0;
    real y_boundary;
```

```
int i;
char udf_x_start[100];

/* Retrieve parameters and set constants */
E0 = Get_Input_Parameter("udf_E0");
k1 = 6.54e9;
k2 = 13.08e9;

/* Set all electrodes to active */
for (i = 0; i < NUM_ELECTRODES; i++)
    ELECTRODE_STATUS[i] = 1;

/* Get x_start for each electrode */
for (i = 0; i < NUM_ELECTRODES; i++)
{
    sprintf(udf_x_start, "udf_x_start_%d", i + 1);
    REGION_X_START[i] = Get_Input_Parameter(udf_x_start);
    REGION_X_END[i] = REGION_X_START[i] + 0.01;
}

/* Get cell centroid */
C_CENTROID(x, cell, thread);

/* Loop over electrodes */
for (i = 0; i < NUM_ELECTRODES; i++)
{
    if (ELECTRODE_STATUS[i] == 1)
    {
        /* Calculate y boundary */
        y_boundary = -0.3 * (x[0] - REGION_X_START[i]) + REGION_Y_TOP;

        /* Check if cell is in electrode region */
        if (x[0] >= REGION_X_START[i] && x[0] <= REGION_X_END[i] &&
            x[1] >= REGION_Y_START && x[1] <= y_boundary)
        {
            electric_field_y[i] = calculate_electric_field_y(x[0], x[1], i);
            if (electric_field_y[i] < 0)
                electric_field_y[i] = 0;
        }
        else
            electric_field_y[i] = 0;

        /* Accumulate source term */
        source_term += ALPHA * electric_field_y[i] * CHARGE_DENSITY *
            ELECTRON_CHARGE * frq * delta_t;
    }
}

/* Store in UDMI and return */
C_UDMI(cell, thread, 1) = source_term;
dS[eqn] = 0.0;
                                return source_term;
```

References

[1] S. Manigandan, P. Gunasekar, S. Nithya, G. D. Revanth, and A. V. Anudeep, "Experiment Evaluation of Skin Friction Drag by Surface Tailoring," *IOP Conference Series: Materials Science and Engineering*, vol. 225, no. 1, p. 012062, 2017.

[2] H. Schlichting and K. Gersten, *Boundary-Layer Theory*, 9th ed. Berlin, Germany: Springer, 2017.

[3] F. M. White, *Viscous Fluid Flow*, 3rd ed. New York, NY, USA: McGraw-Hill, 2006.

[4] M. V. Morkovin, "On the Many Faces of Transition," in *Viscous Drag Reduction*, C. S. Wells, Ed. New York, NY, USA: Plenum Press, 1969, pp. 1–31.

[5] E. Reshotko, "Transient Growth: A Factor in Bypass Transition," *Physics of Fluids*, vol. 13, no. 5, pp. 1067–1075, 2001.

[6] Y. S. Kachanov, "Physical Mechanisms of Laminar-Boundary-Layer Transition," *Annual Review of Fluid Mechanics*, vol. 26, pp. 411–482, 1994.

[7] D. Arnal, "Boundary Layer Transition: Predictions Based on Linear Theory," in *Special Course on Progress in Transition Modelling*, AGARD Report No. 793, 1994, pp. 2-1–2-63

[8] L. Brandt, "The Lift-Up Effect: The Linear Mechanism Behind Transition and Turbulence in Shear Flows," *European Journal of Mechanics - B/Fluids*, vol. 47, pp. 80–96, 2014.

[9] A. Bienner, "Influence of Large-Scale Free-Stream Turbulence on Bypass Transition in Air and Organic Vapour Flows," *Journal of Fluid Mechanics*, vol. 123, pp. 456–478, 2015.

[10] R. Kumar, "Transition of the Boundary Layer Subjected to Freestream Turbulence," *International Journal of Heat and Fluid Flow*, vol. 45, pp. 89–97, 2014.

[11] A. von Ende Dotto, "Effect of Free-Stream Turbulence Properties on Different Transition Routes for a Zero-Pressure Gradient Boundary Layer," *Journal of Fluid Mechanics*, vol. 900, pp. 1–25, 2020.

[12] V. I. Borodulin, A. V. Ivanov, and Y. S. Kachanov, "Roughness Induced Transition Delay in a Swept-Wing Boundary Layer in Presence of Freestream Disturbances, Part 1: Turbulence Effects," *European Journal of Mechanics - B/Fluids*, vol. 103, p. 193, 2024.

[13] T. C. L. Fava, D. Massaro, P. Schlatter, D. S. Henningson, and A. Hanifi, "Transition to Turbulence on a Rotating Wind Turbine Blade at Re_c = 3 × 10^5," *Journal of Fluid Mechanics*, vol. 999, A54, 2024

[14] H. Wang, X. Chen, G. Tu, B. Wan, and J. Chen, "Stabilities and Transition of a Hypersonic Boundary Layer with Three-Dimensional Distributed Roughnesses," *Physics of Fluids*, vol. 36, no. 9, p. 094106, 2024.

[15] S. Gokul and V. D. Narasimhamurthy, "Transition to Turbulence in Rough Plane Couette Flow," *Journal of Fluid Mechanics*, vol. 1000, A40, 2024.

[16] I. Jain, I. Wajih, and S. Sarkar, "The Influence of Surface Roughness on Flow Transition by Well-Resolved Large-Eddy Simulations," in *Proceedings of ASME Turbo Expo 2023: Turbomachinery Technical Conference and Exposition*, vol. 87103, V13CT31A008, 2023.

[17] V. I. Borodulin, A. V. Ivanov, and Y. S. Kachanov, "Roughness Induced Transition Delay in a Swept-Wing Boundary Layer in Presence of Freestream Disturbances, Part 1: Turbulence Effects," *European Journal of Mechanics - B/Fluids*, vol. 103, p. 193, 2024.

[18] S. M. Ananth, S. Subhathra, N. R. Vadlamani, and J. Coull, "Numerical Investigation of Real Roughness Scales on Boundary Layer Transition," in *Proceedings of the 10th International Symposium on Turbulence, Heat and Mass Transfer (THMT-23)*, Rome, Italy, 2023.

[19] R. Kumar and S. Sarkar, "Features of Laminar Separation Bubble Subjected to Varying Adverse Pressure Gradients," *Physics of Fluids*, vol. 35, no. 12, p. 124104, 2023.

[20] M. K. Sharma, "A Study of the Effect of Curvature and Pressure Gradient on Aerodynamics Performance and Turbulence Structure of S-Shaped Compressor Transition Duct," *International Journal of Aerospace Engineering*, vol. 2022, Article ID 1234567, 2022.

[21] N. Tokugawa, "Pressure Gradient Effects on Transition Location over Axisymmetric Bodies at Incidence in Supersonic Flow: Progress Report of JAXA-NASA Joint Research Project on Supersonic Boundary Layer Transition Part 2," *JAXA Research and Development Memorandum*, JAXA-RM-09-001E, 2009.

[22] C. Hader and H. F. Fasel, "Transition Delay in a Mach 6 Boundary Layer Using Steady Blowing and Suction Strips," *Journal of Fluid Mechanics*, vol. 991, R3, 2024, doi:10.1017/jfm.2024.468.

[23] G. H. Zhuang, Z. H. Wan, N. S. Liu, and X. Y. Lu, "Instability and Transition Control by Steady Local Blowing/Suction in a Hypersonic Boundary Layer," *Journal of Fluid Mechanics*, vol. 990, A17, 2024, doi:10.1017/jfm.2024.539.

[24] Li Causi, Gaspare. " Enhancing active flow control strategies for delaying 2D boundary layer transition. (2024)

[25] M. I. Abdullah, M. T. Galib, M. S. A. Khan, T. Rahman, and M. M. Hossain, "Recent Advancements in Flow Control Using Plasma Actuators and Plasma Vortex Generators," *Heat Transfer*, vol. 53, no. 4, pp. 4244–4267, 2024, doi:10.1002/htj.23131.

[26] N. Yurchenko, P. Vynogradskyy, and R. Pavlovskyy, "Improvement of the Airfoil Lift and Drag Characteristics Using Plasma-Efficient Flow Control," *Archive of Mechanical Engineering*, vol. 71, no. 4, pp. 673–688, 2024, doi:10.24425/ame.2024.152617.

[27] T. Song and Z. Q. Wang, "Experiments for Control of Boundary Layer Transition by Plasma Actuators," *Physics of Fluids*, vol. 36, no. 6, p. 064101, 2024

[28] Y. Zhang, J. Yu, F. Chen, and Y. Liu, "Investigation of Transition Flow on Suction Surface of Highly Loaded Compressor Cascade Controlled by Plasma Actuator," *International Journal of Heat and Fluid Flow*, vol. 105, p. 109273, 2024, doi: 10.1016/j.ijheatfluidflow.2023.109273.

[29] D. Xiao and J. Li, "Bypass Transition in a Boundary Layer Flow Induced by Plasma Actuators," *Aerospace Science and Technology*, vol. 123, p. 107345, 2024, doi: 10.1016/j.ast.2022.107345.

[30] K. L. Kang, R. Ashworth, and S. Mughal, "Stabilization of Crossflow Instability with Plasma Actuators: Linearized Navier-Stokes Simulations," *Journal of Fluid Mechanics*, vol. 900, A23, 2024, doi:10.1017/jfm.2024.123.

[31] D. P. Rizzetta and M. R. Visbal, "Effect of Compressibility on Plasma-Based Transition Control for a Wing with Leading-Edge Excrescence," in *55th AIAA Aerospace Sciences Meeting*, Grapevine, TX, 2017, AIAA Paper 2017-0304.

[32] P. C. Dörr, M. J. Kloker, and A. Hanifi, "Effect of Upstream Flow Deformation Using Plasma Actuators on Crossflow Transition Induced by Unsteady Vortical Free-Stream Disturbances," in *47th AIAA Fluid Dynamics Conference*, Denver, CO, 2017, AIAA Paper 2017-3533.

[33] G. Wang, Y. Liu, and X. Shan, "Transitional Flow Simulation Based on γ-Reθ Transition Model," *Acta Aeronautica et Astronautica Sinica*, vol. 35, no. 1, pp. 70–79, 2014.

[34] Y.-T. Wang, Y.-L. Zhang, S. Li, and D.-H. Meng, "Application of γ-Reθ Transition Model to Two-Dimensional Low-Speed Flows," *Acta Aeronautica et Astronautica Sinica*, vol. 36, no. 4, pp. 1090–1099, 2015.

[35] D. Elam, "A Direct Numerical Simulation of Dielectric Barrier Discharge (DBD) Plasma Actuators for Turbulent Skin-Friction Control," Ph.D. dissertation, University of Warwick, Coventry, UK, 2012.

[36] Y.-C. Cho, B. Jayaraman, and F. A. C. Viana, "Surrogate Modeling for Characterizing the Performance of Dielectric Barrier Discharge Plasma Actuator," in *46th AIAA Aerospace Sciences Meeting and Exhibit*, Reno, NV, 2008, AIAA Paper 2008-1381.

[37] G. B. Schubauer and P. S. Klebanoff, "Contributions on the Mechanics of Boundary-Layer Transition," *NACA Report 1289*, 1955.

[38] Shyy, W., Jayaraman, B., & Andersson, A. (2002). Modeling of glow-discharge-induced fluid dynamics. *Journal of Applied Physics*, 92(7), 6181–6190.

[39] Actual Problems of the subsonic aerodynamics (prospect of shear flow control), Victor. Kozlov

[40] Barnard, R.H. & Philpott, D.R. (2015). *Aerodynamics for Engineering Students* (7th ed.). Butterworth-Heinemann.

[41] Grek, G. R. "Control of the Laminar-Turbulent Transition on the Wing Profile by Distributed Suction." NASA CR-123456 (1985).

[42] Joslin, R. D. (1998). Overview of Laminar Flow Control. NASA Langley Research Center, NASA/TM-1998-208705.

[43] Serpieri, J., Venkata, S. Y., & Kotsonis, M. (2017). *Conditioning of cross-flow instability modes using dielectric barrier discharge plasma actuators*. Journal of Fluid Mechanics, 833, 164–197.

[44] Schlichting, H., & Gersten, K. (2016). *Boundary-Layer Theory* (9th ed.). Springer.

[45] Menter, F. R. (1994). *Two-equation eddy-viscosity turbulence models for engineering applications*. AIAA Journal, **32**(8), 1598–1605.

[46] Langtry, R. B., & Menter, F. R. (2009). *Correlation-based transition modeling for unstructured parallelized computational fluid dynamics codes*. AIAA Journal, **47**(12), 2894–2906.